energies

MDPI

Article

Dynamic Response Characteristics Analysis and Energy, Exergy, and Economic (3E) Evaluation of Dual Loop Organic Rankine Cycle (DORC) for CNG Engine Waste Heat Recovery

Baofeng Yao [1,2], Xu Ping [1,2,*] and Hongguang Zhang [1,2]

[1] Key Laboratory of Enhanced Heat Transfer and Energy Conservation of MOE, Faculty of Environment and Life, Beijing University of Technology, Beijing 100124, China; yaobf@bjut.edu.cn (B.Y.); zhanghongguang@bjut.edu.cn (H.Z.)
[2] Beijing Key Laboratory of Heat Transfer and Energy Conversion, Faculty of Environment and Life, Beijing University of Technology, Beijing 100124, China
* Correspondence: pxpingxu@163.com

Abstract: Frequent fluctuations of CNG engine operating conditions make the waste heat source have uncertain, nonlinear, and strong coupling characteristics. These characteristics are not conducive to the efficient recovery of the DORC system. The systematic evaluation of the CNG engine waste heat source and the comprehensive performance of the DORC system is conducive to the efficient use of waste heat. Based on the theory of internal combustion (IC) engine thermal balance, this paper analyzes the dynamic characteristics of compressed natural gas (CNG) engine waste heat energy under full operating conditions. Then, based on the operating characteristics of the dual loop organic Rankine cycle (DORC) system, thermodynamic models, heat transfer models, and economic models are constructed. The dynamic response characteristics analysis and energy, exergy, and economic (3E) evaluation of the DORC system under full operating conditions are carried out. The results show that the maximum values of net power output, heat exchange area, and the minimum values of EPC (electricity production cost) and PBT (payback time) are all obtained under rated condition, which are 174.03 kW, 25.86 kW, 37.54 kW, 24.76 m^2, 0.15 \$/kW·h and 3.46 years. Therefore, the rated condition is a relatively ideal design operating point for the DORC system. The research in this paper not only provides a reliable reference for the comprehensive analysis and evaluation of the performance of the DORC system, but also provides useful guidance for the selection of appropriate DORC system design operating points.

Keywords: CNG engine; waste heat recovery; dual loop organic Rankine cycle; dynamic response characteristics; full operating conditions

Citation: Yao, B.; Ping, X.; Zhang, H. Dynamic Response Characteristics Analysis and Energy, Exergy, and Economic (3E) Evaluation of Dual Loop Organic Rankine Cycle (DORC) for CNG Engine Waste Heat Recovery. *Energies* **2021**, *14*, 6224. https://doi.org/10.3390/en14196224

Academic Editor: Constantine D. Rakopoulos

Received: 27 August 2021
Accepted: 24 September 2021
Published: 29 September 2021

1. Introduction

Oil used as a fuel plays an important role in the development of society and the economy. In the field of oil consumption, the power industry, dominated by internal combustion (IC) engines, occupies a large proportion [1]. Because of its easy access, abundant output, low price, and environmental friendliness, compressed natural gas (CNG) has been widely proposed as an alternative fuel for IC engines [2,3]. Analyzing the energy distribution from the perspective of internal combustion engine thermal balance, it can be found that only part of the energy is converted into useful work, and the remaining energy is mainly lost in the form of waste heat [4]. As a clean and efficient power cycle, the organic Rankine cycle (ORC) can effectively recover and utilize the waste heat of IC engines, thereby improving the fuel economy [5,6]. The dual loop organic Rankine cycle (DORC) system can realize the efficient recovery and utilization of different types of waste heat sources of IC engines [7].

Compared with marine engines and stationary IC engines with relatively stable waste heat energy, the variable operating conditions of vehicle IC engines have led to the

complexity and variability of the waste heat energy [8]. Due to the frequent changes in operating conditions of IC engines for vehicles, the organic Rankine cycle (ORC) system cannot have enough work capacity under most operating conditions of IC engines. The actual thermal efficiency of the ORC system was 3.67% (the thermal efficiency of the system under design condition was 7.77%) [9]. Under the New York City Cycle road condition, the exhaust heat energy fluctuated frequently and the energy was low; under the Common Artemis Driving Cycles road condition, the exhaust heat energy fluctuated little and the energy was high [10]. The exhaust temperature of the IC engines under heavy load was more than 300 K higher than the exhaust temperature under light load; the exhaust mass flow rate under heavy load was more than three times higher than that under light load [11]. Moreover, the energy grades of the intercooler waste heat energy, the jacket water waste heat energy (353.15–373.15 K) and the exhaust waste heat energy (673.15–1173.15 K) were different [12]. Therefore, the characteristics of high frequency and wide variation range of the waste heat sources of IC engines bring great challenges to the efficient operation of the DORC system. Full operating conditions refer to all operating conditions of the CNG engine and all operating conditions of the ORC system. The analysis and evaluation of the CNG engine waste heat sources under full operating conditions are beneficial to the stable operation of the DORC system.

The complex and variable waste heat characteristics of IC engines affected the dynamic response characteristics of the DORC system [13]. A simplified diagram of the DORC system is shown in Figure 1. The reduction of the waste heat energy of the IC engine reduces the evaporation pressure, power output, and mass flow rate in the loop. Compared with the condensation pressure in the HT loop, the condensation pressure drop of the LT loop is smaller. Moreover, the decrease of power output in LT loop is significantly higher than that in HT loop [14]. In addition, the IC engine waste heat sources has an important influence on the evaporation temperature in the HT loop, and an appropriate increase in the evaporation temperature of the HT loop is conducive to improving the operating performance of the system [15]. To sum up, analyzing and evaluating the dynamic response characteristics of the DORC system under full operating conditions of the CNG engine will help to obtain comprehensive waste heat recovery performance [16]. Table 1 briefly lists the selection of operating conditions when recovering waste heat from IC engine in recent years [17–29]. It can be seen from the table that researchers have carried out a lot of research on ORC systems from different perspectives, but most of them use constant heat source (usually the rated condition of engine) as the high-temperature heat source for the ORC system. This choice will lead to insufficient evaluation of the performance of the ORC system under full operating conditions. Moreover, when evaluating and analyzing system operating performance, most researchers focus on the impact of operating parameters on system performance. From the above analysis, it can be seen that the characteristics of the waste heat sources of IC engines under different operating conditions have an important impact on the operating performance of the DORC system, and the impacts are significantly different.

In addition, due to the large temperature gradient characteristic of the waste heat energy of IC engines, the operating conditions of the CNG engines significantly affect the operating performance of DORC. Therefore, it is particularly important to evaluate the performance of the DORC system under full operating conditions of the IC engines [30,31]. Table 2 simply lists the indicators used to evaluate the operating performance of ORC systems in recent years [32–43]. It can be seen from the table that only a few indicators are selected to evaluate the performance of the ORC system. As a result, the operating performance of the ORC system has not been fully evaluated. Moreover, it does not fully consider the impact of the IC engine on the operating performance of the system under variable operating conditions. In addition the operating performance of different components of the DORC system also has an important impact on the performance of the system. The evaporator in HT loop and the condenser in LT loop are the two components with the largest exergy destruction in the system [44]. In addition, under different operating

conditions of the IC engine, the operating performance of the system components has obvious differences in the impact of the overall operating performance [45]. Therefore, for the DORC system for CNG engine WHR, it is particularly important to analyze the operating performance of HT loop, LT loop, and different components to comprehensively evaluate the system performance.

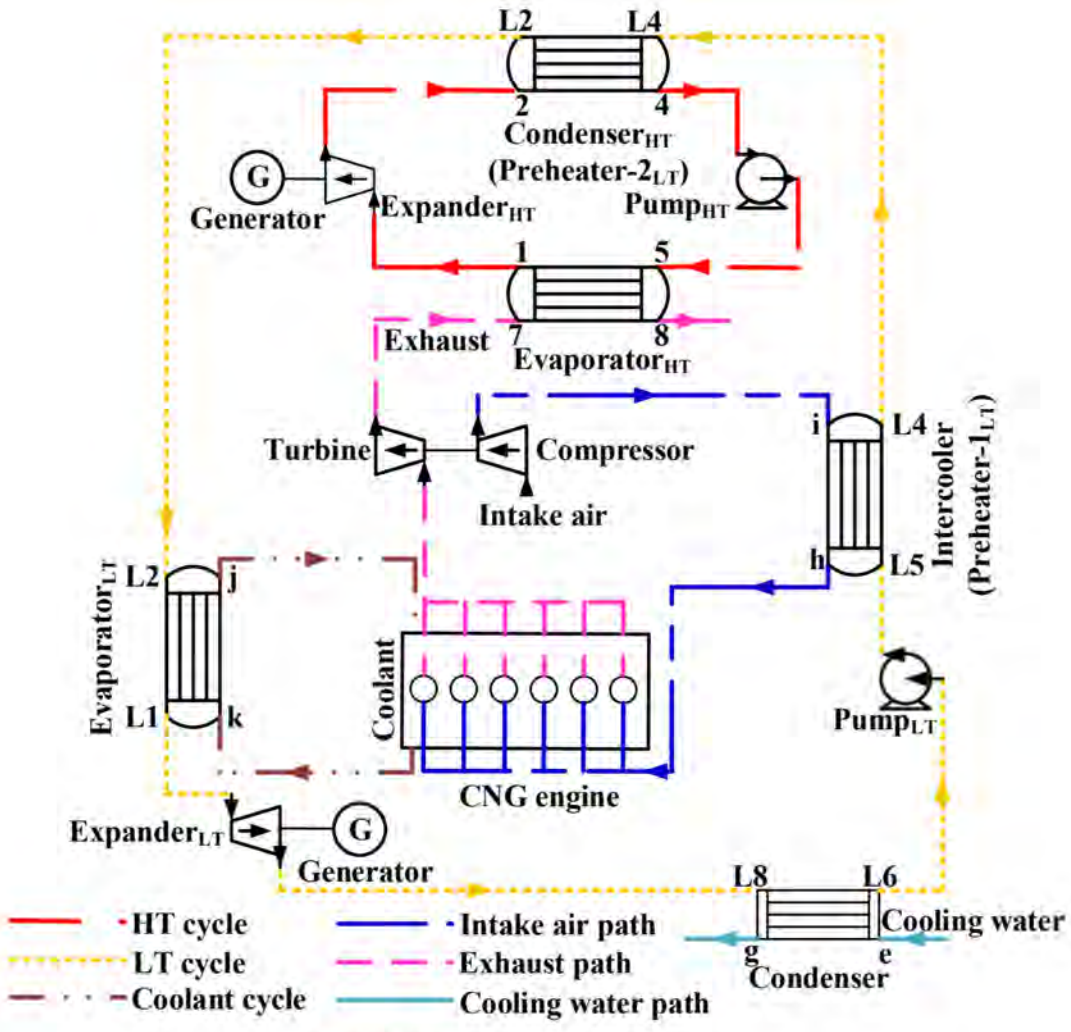

Figure 1. Schematic of the DORC system.

Table 2 shows ORC systems in recent years [32–43]. It can be seen from the table that only a few indicators are selected to evaluate the performance of the ORC system. As a result, the operating performance of the ORC system has not been fully evaluated. Moreover, it does not fully consider the impact of the IC engine on the operating performance of the system under variable operating conditions. In addition, the operating performance of different components of the DORC system also has an important impact on the performance of the system. The evaporator in HT loop and the condenser in LT loop are the two components with the largest exergy destruction in the system [44]. In addition, under different operating conditions of the IC engine, the operating performance of the system components has obvious differences in the impact of the overall operating performance [45]. Therefore, for the DORC system for CNG engine WHR, it is particularly important to analyze the operating performance of HT loop, LT loop, and different components to comprehensively evaluate the system performance.

Table 1. Selection of operating conditions of IC engine.

Refs.	Year	Research Description	Waste Heat Sources
Baldasso et al. [17]	2020	Optimal design of ORC system for marine engine WHR based on performance maps, numerical models, and waste heat recovery boiler.	Engine power output: 23 MW; engine speed: 74 r/min; exhaust temperature: 524.15 K; exhaust mass flow rate: 51.9 kg/s
Wang et al. [18]	2020	Selection of working fluid used in DORC for engine WHR based on thermo-economic selection criteria.	Engine power output: 235.8 kW; exhaust temperature: 792.15 K; exhaust mass flow rate: 0.275 kg/s
Zhi et al. [19]	2020	Based on mathematical stepwise searching method, the operating performance of transcritical-subcritical parallel organic Rankine cycle was optimized.	Engine power output: 996 kW; engine speed: 1500 r/min; engine torque: 6340 N·m; exhaust temperature: 573.15 K; exhaust mass flow rate: 1.91 kg/s
Zhi et al. [20]	2020	The energy and exergy analysis of transcritical CO2 parallel Rankine cycle for engine WHR were analyzed.	Engine power output: 996 kW; engine speed: 1500 r/min; engine torque: 6340 N·m; exhaust temperature: 573.15 K; exhaust mass flow rate: 1.91 kg/s
Song et al. [21]	2020	The parameters of the supercritical CO2-ORC system for engine WHR were optimized from the perspective of thermodynamics and economy.	Engine power output: 1170 kW; exhaust temperature: 730.15 K; exhaust mass flow rate: 1.69 kg/s
Zhi et al. [22]	2019	The energy, exergy, and design parameters of transcritical-subcritical parallel organic Rankine cycle for engine WHR were analyzed.	Engine power output: 996 kW; engine speed: 1500 r/min; engine torque: 6340 N·m; exhaust temperature: 573.15 K; exhaust mass flow rate: 1.98 kg/s
Fang et al. [23]	2019	The thermodynamic and thermal-economic performance of ORC system with pure working fluids and their zeotropic mixtures for engine WHR were compared.	Engine power output: 247 kW; engine speed: 1900 r/min; engine torque: 1243 N·m; exhaust temperature: 653.15 K; exhaust mass flow rate: 0.36 kg/s
Mat Nawi et al. [24]	2019	The potential of ORC system for marine diesel engine WHR was analyzed.	Engine power output: 996 kW; engine speed: 1500 r/min; engine torque: 6340 N·m; exhaust temperature: 573.15 K; exhaust mass flow rate: 1.98 kg/s
Shu et al. [25]	2017	The dynamic response characters of ORC system with different working fluids for engine WHR were analyzed.	Engine power output: 1000 kW; engine speed: 600 r/min; exhaust temperature: 813.15 K; exhaust mass flow rate: 1.56 kg/s
Chen et al. [26]	2017	The operating performance of the confluent cascade expansion ORC system for diesel engine waste heat recovery is analyzed.	Engine power output: 258.9 kW; engine speed: 1400 r/min; exhaust temperature: 678.15 K; exhaust mass flow rate: 0.388 kg/s
Seyedkavoosi et al. [27]	2017	The exergy of two-parallel-step ORC system for engine WHR was analyzed. In addition, a thermodynamic model was constructed and the operating performance was optimized.	Engine power output: 2928 kW; engine speed: 1000 r/min; exhaust temperature: 743.15 K; exhaust mass flow rate: 4.35 kg/s
Kim et al. [28]	2016	The performance of novel single-loop ORC system for engine WHR was analyzed, and was compared to the performance of conventional single-loop system.	Engine power output: 26.7 kW; engine torque: 106.2 N·m; engine speed: 2400 r/min; exhaust temperature: 962.15 K
de Oliveira Neto et al. [29]	2016	The applicability of the ORC system for engine WHR was analyzed and the economics of ORC system were analyzed.	Engine power output: 830 kW; exhaust temperature: 746.35 K; exhaust mass flow rate: 0.0014 kg/s

Table 2. Selection of ORC system operation performance index.

Refs.	Year	Research Description	Performance Evaluation Index
Wang et al. [32]	2021	The selection of working fluid and exergy analysis of DORC system were conducted.	Exergy efficiency Payback period Annual CO_2 emission reduction
Fouad et al. [33]	2020	The operating performance of DORC system for biomass gasification WHR was analyzed.	Net power output Thermal efficiency Exergy efficiency
Linnemann et al. [34]	2020	The operating performance of the two cascaded ORC system for power plant WHR was designed and tested.	Net power output Thermal efficiency
Liu et al. [35]	2020	Through Rankine cycle, ORC and absorption refrigeration cycle, the waste heat of marine engines was recovered, and the thermodynamic performance of the system was evaluated.	Net power output Thermal efficiency
Surendran et al. [36]	2020	The operating performance of Series two stage ORC and parallel two stage ORC for engine WHR was compared and analyzed.	Net power output Thermal efficiency Exergy efficiency
Ebadollahi et al. [37]	2020	First, ORC and vapor compressor refrigeration cycle were coupled into an integrated system, and then IHE and FFH were applied to the ORC loop. In addition, the operation performance of the system was analyzed from the perspective of thermodynamics and exergy.	Net power output Thermal efficiency Exergy efficiency Exergy destruction
Pourpasha et al. [38]	2020	A hybrid DORC-Generator absorber exchange cycle for WHR was designed, and the operating performance of the system was analyzed and evaluated.	Exergy efficiency Thermal efficiency Exergy destruction Exergy destruction ratio Net power output
Emadi et al. [39]	2020	The operating performance of DORC for waste heat recovery of solid oxide fuel cell system equipped with gas turbine was analyzed and optimized.	Cost rate Exergy efficiency
Xia et al. [40]	2020	The working fluid of the DORC system was selected.	Exergy efficiency Payback period Annual CO_2 emission reduction
Mohammadkhani et al. [41]	2019	The operating performance of the DORC system for diesel engine WHR was analyzed. In addition, the working fluid was selected.	Net power output Thermal efficiency Payback period Investment cost
Ouyang et al. [42]	2019	A combined system with DORC, absorption refrigeration, and flue gas purification for WHR was modeled, and the performance of the system was evaluated.	Net power output Thermal efficiency Exergy destruction Exergy efficiency
Liang et al. [43]	2019	The operating performance of the regenerative super-critical carbon dioxide Brayton cycle/ORC dual loop for dual-fuel engine WHR was analyzed and evaluated.	Net power output Energy efficiency Exergy efficiency Exergy loss

Based on the theory of IC engine heat balance in high-dimensional space, this paper first analyzes the dynamic characteristics of CNG engine exhaust, intercooler, and coolant

waste heat sources under full operating conditions. Then, the proportion of different waste heat energy in fuel energy is evaluated. In addition, based on the operating characteristics of the DORC system, the thermodynamic model, heat transfer model, and economic model of the system are constructed, respectively. In the high-dimensional space, the thermal efficiency, total exergy destruction, net power output, heat exchange area, POPA (net power output per unit heat transfer area), EPC (electricity production cost), PBT (payback time), and total investment cost of the DORC system under full operating conditions of the CNG engine are analyzed. Based on the operating characteristics of different loops in the system, the thermodynamic model, heat transfer model, and economic model of the HT and LT loop are constructed respectively. In the high-dimensional space, the exergy destruction, net power output, heat exchange area, and POPA of the HT and LT loop under the full operating conditions of the CNG engine are analyzed. Based on the operating characteristics of the key components in the system, thermodynamic models, heat transfer models, and economic models of different components are constructed. In the high-dimensional space, the exergy destruction and investment cost of the key components of the DORC system under full operating conditions of the CNG engine are analyzed. In addition, the proportion of exergy destruction and investment cost of key components are analyzed respectively.

2. CNG Engine Waste Heat Characteristics

Part of the heat energy is lost due to heat radiation. Radiation losses are relatively small, so they may not be taken into account. In CNG engine, only part of the energy completely released by fuel combustion is converted into useful work, while the rest of the energy is lost through exhaust and cooling water. This paper obtains the distribution of useful work and various energy losses through the engine heat balance theory, so as to evaluate the WHR potential of the CNG engine.

In the energy balance equation, the energy released by fuel combustion is determined by the low heating value of the fuel and the fuel consumption obtained through measurement. The useful work is obtained by the dynamometer. The exhaust energy is determined by the engine exhaust temperature, specific heat, and exhaust mass flow rate. The waste heat of coolant is determined by the measured coolant mass flow rate, the coolant inlet temperature, and the coolant outlet temperature. The waste heat of intercooler is determined by the measured intercooler mass flow rate, the intercooler inlet temperature, and the intercooler outlet temperature. The main parameters of CNG engine are shown in Table 3.

Table 3. Main parameters of engine.

Property	Value	Unit
Cylinder number	6	-
Stroke and cylinder bore	114 × 144	mm
Maximum torque	1120	N·m
Low calorific value	44.7	$MJ/N \cdot m_n^3$
Displacement	8.9	L
Rated power	210	kW
Rated speed	2200	r/min

The CNG engine heat balance equation is:

$$Q_{exh} + \dot{W}_{eng} + Q_{cool} + Q_{inter} + Q_{env} = Q_{tot} \quad (1)$$

where,

the calculation formula of CNG engine intercooler heat transfer rate:

$$\dot{Q}_{inter} = \dot{m}_{inter} C_{p_{air}} (T_{inter,in} - T_{inter,out}) \quad (2)$$

the calculation formula of CNG engine coolant heat transfer rate:

$$\dot{Q}_{\text{cool}} = \dot{m}_{\text{cool}} C_{p_{\text{cool}}} (T_{\text{cool,out}} - T_{\text{cool.in}}) \tag{3}$$

the calculation formula of CNG engine exhaust heat transfer rate:

$$\dot{Q}_{\text{exh}} = \dot{m}_{\text{exh}} (h_{\text{exh,in}} - h_{\text{exh,out}}) \tag{4}$$

In addition, the energy of different waste heat sources accounted for the proportion of energy released by fuel combustion under full operating conditions. In the high-dimensional space, the characteristics of the waste heat sources are analyzed.

2.1. Exhaust Waste Heat

Figure 2 shows the dynamic characteristics of CNG engine exhaust heat source under full operating conditions. Figure 2a shows the exhaust mass flow rate distribution characteristics under full operating conditions. It can be seen from the figure that as the speed increases, the exhaust mass flow rate gradually increases; and in high torque range, the exhaust mass flow rate increases significantly. As the torque increases, the exhaust mass flow rate gradually increases; and in high speed range, the exhaust mass flow rate increases significantly. The high exhaust mass flow rate is distributed near the rated condition. The maximum exhaust mass flow rate is obtained under the rated condition, which is 0.3 kg/s. Figure 2b shows the exhaust heat transfer rate distribution characteristics under full operating conditions. It can be seen from the figure that the change trend of exhaust heat transfer rate with speed and torque is similar to that of exhaust mass flow rate. The high exhaust heat transfer rate is distributed near the rated condition, but it is narrower than the exhaust mass flow rate distribution area. The maximum exhaust heat transfer rate is obtained under the rated condition, which is 174.03 kW. Figure 2c shows the proportion of exhaust heat transfer rate to the energy released by fuel combustion under full operating condition. It can be seen from the figure that as the speed increases, the proportion of exhaust heat transfer rate gradually increases. With the increase of torque, the proportion of exhaust heat transfer rate increases, but the increase is not obvious. Compared with torque, speed has a greater influence on the proportion of exhaust heat transfer rate. The proportion of high heat transfer rate is distributed in high speed range.

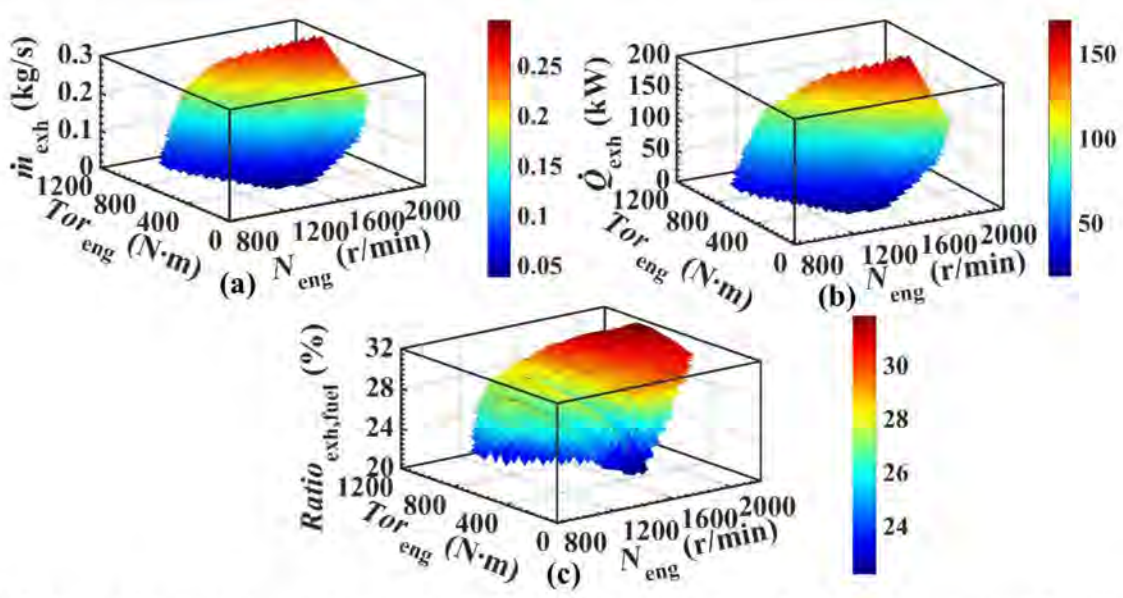

Figure 2. Dynamic characteristics of exhaust waste heat under full operating conditions. (**a**) exhaust mass flow rate distribution characteristics under full operating conditions. (**b**) exhaust heat transfer rate distribution characteristics. (**c**) proportion of exhaust heat transfer rate to the energy released by fuel combustion.

2.2. Intercooler Waste Heat

Figure 3 shows the dynamic characteristics of CNG engine intercooler heat source under full operating conditions. Figure 3a shows the intercooler mass flowrate distribution characteristics under full operating conditions. It can be seen from the figure that as the speed increases, the intercooler mass flow rate gradually increases; and in high torque range, the intercooler mass flow rate increases significantly. As the torque increases, the intercooler mass flow rate gradually increases; and in high speed range, the intercooler mass flow rate increases significantly. The intercooler mass flow rate is distributed near the rated condition. The maximum intercooler mass flow rate is obtained under the rated condition, which is 0.29 kg/s. Figure 3b shows the intercooler heat transfer rate distribution characteristics under full operating conditions. It can be seen from the figure that the change trend of intercooler heat transfer rate with the speed and torque is similar to that of intercooler mass flow rate. The high intercooler heat transfer rate is distributed near the rated condition, but it is narrower than the intercooler mass flow rate distribution area. In the high intercooler heat transfer rate area, the range covered by the torque is larger than the speed. The maximum intercooler heat transfer rate is obtained under the rated condition, which is 25.86 kW. Figure 3c shows the proportion of the intercooler heat transfer rate to the energy released by fuel combustion under full operating conditions. It can be seen from the figure that as the speed increases, the proportion of the intercooler heat transfer rate gradually increases; at the same time, as the torque increases, the increase gradually flat. As the torque increases, the proportion of the intercooler heat transfer rate gradually increases; at the same time, as the speed increases, the increase gradually flattens. Speed and torque have similar effects on the proportion of intercooler heat transfer rate. The proportion of the high heat transfer rate is distributed in high speed, high torque range.

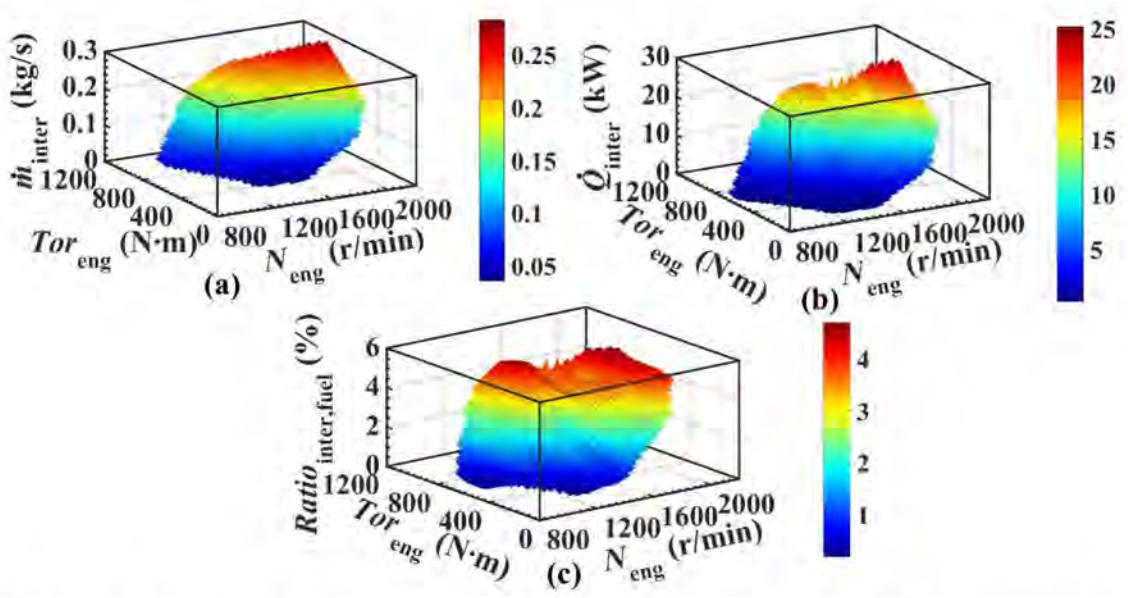

Figure 3. Dynamic characteristics of intercooler waste heat under full operating conditions. (**a**) intercooler mass flowrate distribution characteristics. (**b**) intercooler heat transfer rate distribution characteristics. (**c**) proportion of the intercooler heat transfer rate to the energy released by fuel combustion.

2.3. Coolant Waste Heat

Figure 4 shows the dynamic characteristics of the CNG engine coolant heat source under full operating conditions. Figure 4a shows the distribution characteristics of the coolant mass flow rate under full operating conditions. It can be seen from the figure that as the speed increases, the coolant mass flow rate gradually increases. With the increase of torque, the change of coolant mass flow rate is not obvious. The high coolant mass flow rate is distributed in the high speed range. Figure 4b shows the coolant heat transfer

rate distribution characteristics under full operating conditions. It can be seen from the figure that as the speed increases, the coolant heat transfer rate gradually increases; but as the speed increases, the increase of the coolant heat transfer rate gradually decreases. As the torque increases, the coolant heat transfer rate generally increases, but the increase is not obvious. The high coolant heat transfer rate is distributed in high speed range. Figure 4c shows the proportion of the coolant heat transfer rate to the energy released by fuel combustion under full operating conditions. Under the engine rated condition, the mass flow rate and heat transfer amount of the coolant are 3.74 kg/s and 100.49 kW, respectively. It can be seen from the figure that with the increase of speed, the change of coolant heat transfer rate is not obvious. With the increase of torque, the proportion of the coolant heat transfer rate gradually decreases; and with the increase of torque, the decrease gradually flat. Compared with speed, torque has a greater influence on the proportion of coolant heat transfer rate. The proportion of high coolant heat transfer rate is distributed in low torque range.

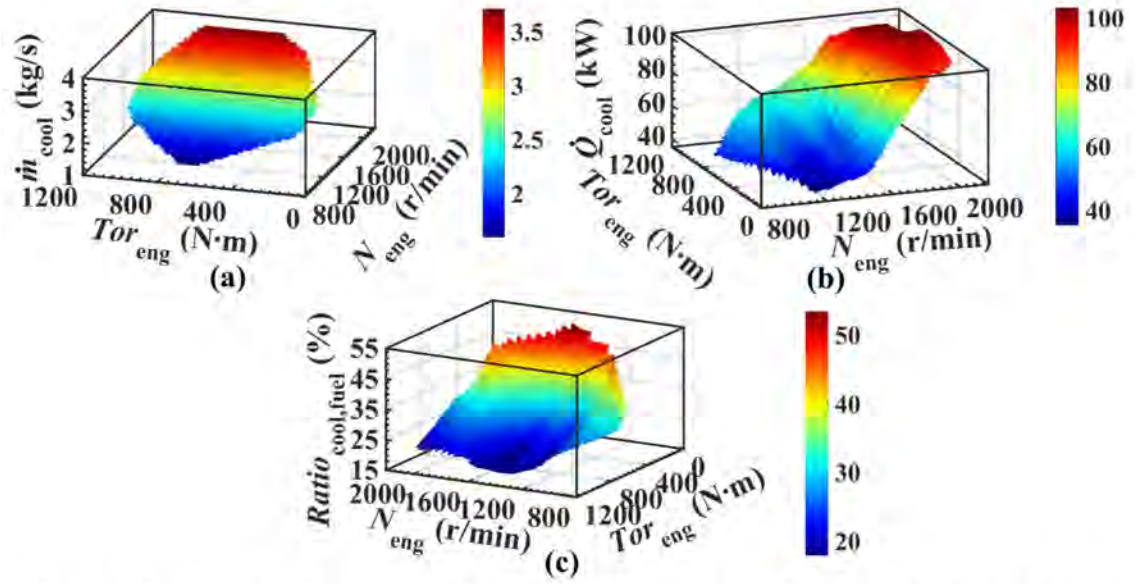

Figure 4. Dynamic characteristics of coolant waste heat under full operating conditions. (**a**) distribution characteristics of the coolant mass flow rate. (**b**) coolant heat transfer rate distribution characteristics. (**c**). proportion of the coolant heat transfer rate to the energy released by fuel combustion.

3. DORC Model

3.1. System Description

Figure 1 shows the schematic of the DORC system. From the figure, the HT loop and LT loop constitute the main loop of the DORC system. CNG engine exhaust waste heat is mainly recovered by HT loop. After the working fluid in HT loop exchanges heat with the exhaust in evaporator, it becomes high-temperature and high-pressure vapor. Then it enters the expander to do work. The vapor after the work enters the preheater and exchanges heat with the working fluid in LT loop, and becomes saturated liquid. Finally, it is pressurized by the working fluid pump and enters the evaporator again for heat exchange. The T-s diagram of HT loop is shown in Figure 5. The T-s diagram of LT loop is shown in Figure 6. CNG engine intercooler waste heat and coolant waste heat are mainly recovered by LT loop. The working fluid in LT loop sequentially exchanges heat in the intercooler and the preheater, and then enters the evaporator for heat exchange. It becomes saturated steam and enters the expander, pushing the expander to do work. The vapor after work enters the condenser and becomes saturated liquid. Then it is pressurized by the working fluid pump and enters the LT loop again.

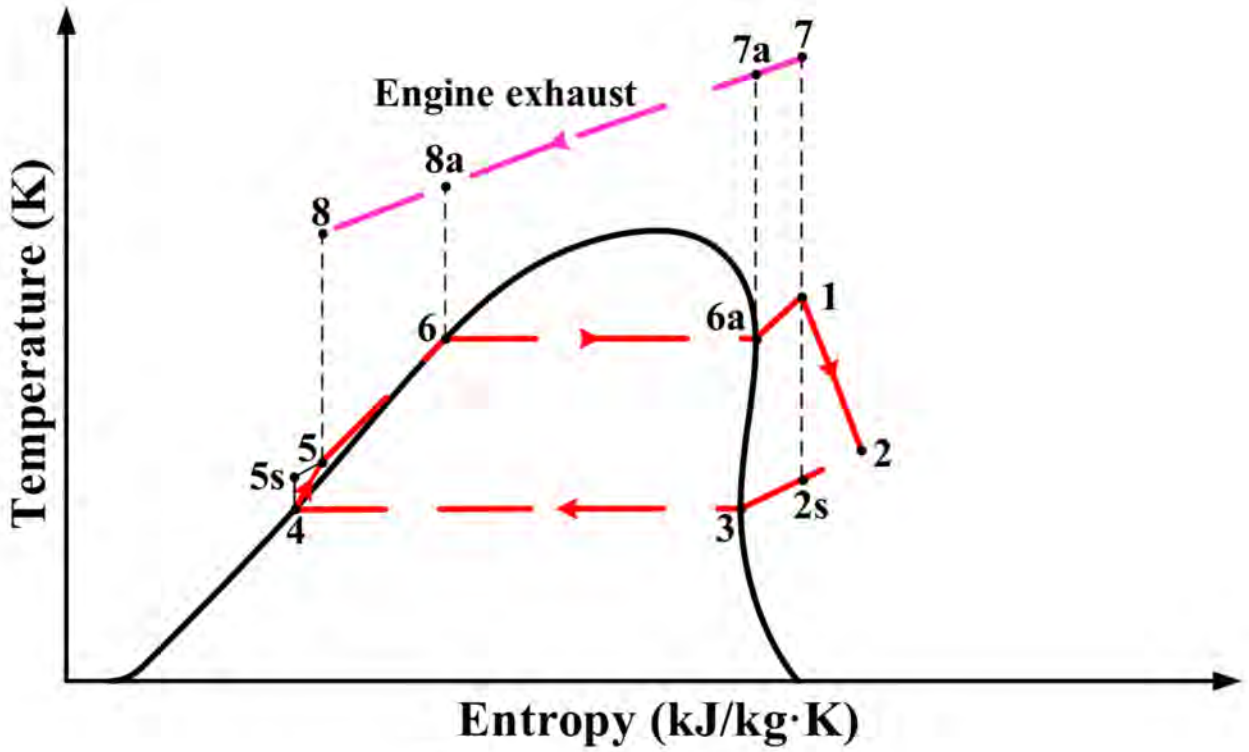

Figure 5. HT loop of the DORC system.

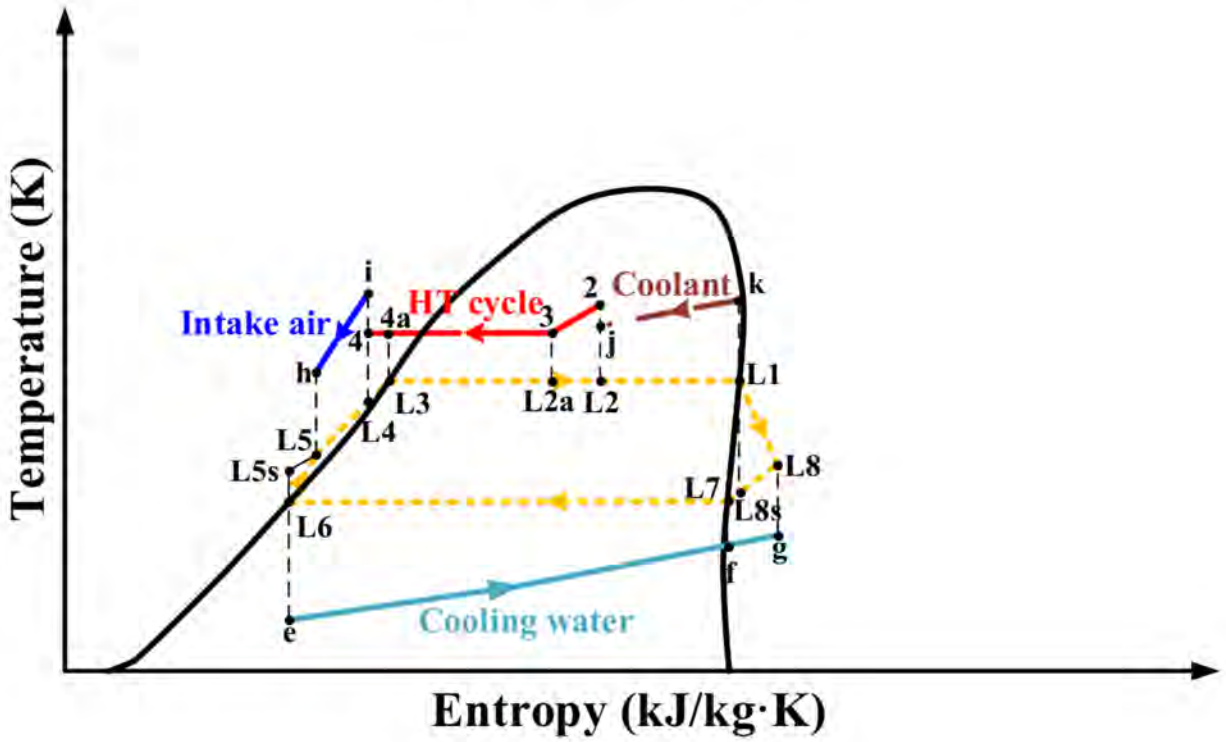

Figure 6. LT loop of the DORC system.

R245fa can be regarded as an isentropic working fluid in some temperature ranges. Compared with wet working fluid, isentropic working fluid is more suitable for ORC system. This is because the wet working fluid will be condensed during the expansion process, which makes the outlet working fluid of the expander appear in a gas-liquid two-phase

state, resulting in a liquid hammer phenomenon in the expander [46–48]. Moreover, R245fa has shown good performance in the application of ORC system and is widely used in ORC experimental system [49,50]. Therefore, R245fa is selected as the working fluid of HT cycle and LT loop.

3.2. Thermodynamic Model

The DORC system consists of HT loop and LT loop. The HT loop includes four processes: expansion, condensation, compression, and evaporation. The expansion process in HT loop is 1–2. The power output of the expander ($\dot{W}_{exp,HT}$) can be defined as:

$$\dot{W}_{exp,HT} = \dot{m}_{wf,HT}(h_1 - h_2) \tag{5}$$

The isentropic efficiency of the expansion process ($\eta_{exp,HT}$) can be defined as [51]:

$$\eta_{exp,HT} = \frac{h_1 - h_2}{h_1 - h_{2s}} \tag{6}$$

The heat transfer rate of preheater ($\dot{Q}_{pre,HT}$) can be defined as:

$$\dot{Q}_{pre,HT} = \dot{m}_{wf,HT}(h_2 - h_4) \tag{7}$$

The pressurization process of the working fluid pump in HT loop is 4–5. The power consumption of the working fluid pump during the pressurization process ($\dot{W}_{p,HT}$) can be defined as [52]:

$$\dot{W}_{p,HT} = \dot{m}_{wf,HT}(h_5 - h_4) \tag{8}$$

The isentropic efficiency of the pressurization process ($\eta_{p,HT}$) can be defined as:

$$\eta_{p,HT} = \frac{h_{5s} - h_4}{h_5 - h_4} \tag{9}$$

In HT loop, the heat absorption process of the working fluid in evaporator is 5–1. The heat transfer rate of the evaporator ($\dot{Q}_{eva,HT}$) can be defined as:

$$\dot{Q}_{eva,HT} = \dot{m}_{wf,HT}(h_1 - h_5) = \dot{m}_{exh}(h_7 - h_8) \tag{10}$$

In addition, the net power output in HT loop ($\dot{W}_{net,HT}$) can be defined as [53]:

$$\dot{W}_{net,HT} = \dot{W}_{exp,HT} - \dot{W}_{p,HT} \tag{11}$$

Similar to the thermodynamic process of the HT loop, the LT loop also includes four processes of expansion, condensation, compression and evaporation. The expansion process in LT loop is L1–L8. The power output of the expander ($\dot{W}_{exp,LT}$) can be defined as:

$$\dot{W}_{exp,LT} = \dot{m}_{wf,LT}(h_{L1} - h_{L8}) \tag{12}$$

The isentropic efficiency of the expansion process ($\eta_{exp,LT}$) can be defined as [54]:

$$\eta_{exp,LT} = \frac{h_{L1} - h_{L8}}{h_{L1} - h_{L8s}} \tag{13}$$

In LT loop, the heat release process in the condenser is L8–L6. The heat transfer rate of the condenser ($\dot{Q}_{con,LT}$) can be defined as:

$$\dot{Q}_{con,LT} = \dot{m}_{wf,LT}(h_{L8} - h_{L6}) \tag{14}$$

The pressurizing process of the working fluid pump in LT loop is L6–L5. The power consumption of the working fluid pump during the pressurization process ($\dot{W}_{p,LT}$) can be defined as:

$$\dot{W}_{p,LT} = \dot{m}_{wf,LT}(h_{L5} - h_{L6}) \quad (15)$$

The isentropic efficiency of the pressurization process ($\eta_{p,LT}$) can be defined as [55]:

$$\eta_{p,LT} = \frac{h_{L5s} - h_{L6}}{h_{L5} - h_{L6}} \quad (16)$$

In LT loop, the heat absorption process of the working fluid in intercooler is L5–L4. The heat transfer rate of the intercooler ($\dot{Q}_{inter}$) can be defined as:

$$\dot{Q}_{inter} = \dot{m}_{wf,LT}(h_{L4} - h_{L5}) = \dot{m}_{inter}(h_i - h_h) \quad (17)$$

In LT loop, the heat absorption process of the working fluid in preheater is L4–L2. The heat transfer rate of the preheater ($\dot{Q}_{pre,LT}$) can be defined as [56]:

$$\dot{Q}_{pre,LT} = \dot{m}_{wf,LT}(h_{L2} - h_{L4}) \quad (18)$$

In LT loop, the heat absorption process of the working fluid in evaporator is L2–L1. The heat transfer rate of the evaporator can be defined as:

$$\dot{Q}_{eva,LT} = \dot{m}_{wf,LT}(h_{L1} - h_{L2}) \quad (19)$$

In addition, the net power output in LT loop can be defined as:

$$\dot{W}_{net,LT} = \dot{W}_{exp,LT} - \dot{W}_{p,LT} \quad (20)$$

For the DORC:

The net power output of the DORC ($\dot{W}_{net}$) can be defined as [57]:

$$\dot{W}_{net} = \dot{W}_{net,HT} + \dot{W}_{net.LT} \quad (21)$$

The thermal efficiency of the DORC (η_{th}) can be defined as:

$$\eta_{th} = 100\% \times \frac{\dot{W}_{net}}{Q_{eva,HT} + Q_{int} + Q_{eva,LT}} \quad (22)$$

3.3. Heat Transfer Model

The heat exchange process of the DORC system is completed by multiple heat exchangers, and the heat exchange process is complex and changeable. The heat transfer process of the system is analyzed by constructing the heat transfer model. Fin-and-tube heat exchanger is suitable for high-temperature and high-pressure sources. Plate heat exchanger is suitable for low-temperature heat source because of its low cost and easy maintenance. Therefore, the fin-and-tube heat exchanger is selected as the evaporator in HT loop; The rest of the heat exchangers in HT loop and LT loop are plate heat exchangers. The main parameters of the fin-and-tube heat exchanger and plate heat exchanger used are shown in Table 4.

Table 4. Main parameters of exchangers.

Property	Value	Unit
	Fin-and-tube heat exchanger	
Tube outer diameter	25	mm
Tube inner diameter	20	mm
Fin height	12	mm
Fin width	1	mm
Tube length	8.8	m
Tube pitch	60	mm
Row pitch	100	mm
	Plate heat exchanger	
Plate thickness	0.35	mm
Plate length	0.536	m
Plate width	0.123	m
Corrugation width	4	mm
Corrugation depth	3	mm

In this paper, the heat exchange process of the fin-and-tube heat exchanger is simplified into the preheating section, the two-phase section and the overheating section; According to different heat exchange processes, the heat exchange process of the condenser is simplified into the preheating section, the two-phase section, the superheating section and the condensation section [58,59]. The heat transfer model of the DORC system is constructed by the logarithmic mean temperature difference (LMTD) method. The heat transfer rate can be defined as [60,61]:

$$\dot{Q} = AK\Delta T_{\mathrm{LMTD}} \tag{23}$$

In the equation ΔT_{LMTD} can be defined as:

$$\Delta T_{\mathrm{LMTD}} = \frac{\Delta t_{\max} - \Delta t_{\min}}{\ln \frac{\Delta t_{\max}}{\Delta t_{\min}}} \tag{24}$$

The heat transfer model construction process of fin-and-tube heat exchanger is:
The total heat transfer coefficient (K_{ft}) can be defined as:

$$\frac{1}{K_{\mathrm{ft}}} = \frac{\beta}{\alpha_{\mathrm{in}}} + r_{\mathrm{in}}\beta + \frac{\delta\beta}{\lambda} + \frac{r_{\mathrm{out}}}{\eta_{\mathrm{f}}} + \frac{1}{\alpha_{\mathrm{out}}\eta_{\mathrm{f}}} \tag{25}$$

where,

$$\alpha = \frac{\lambda Nu}{d} \tag{26}$$

The formula for calculating the Nusselt number on the exhaust side is determined by the Zhukauskas correlation equation [62]:

$$Nu_{\mathrm{exh}} = 0.35\varepsilon^{0.2} Re_{\mathrm{exh}}^{0.6} Pr_{\mathrm{exh}}^{0.36} \left(\frac{Pr_{\mathrm{exh}}}{Pr_{\mathrm{exh,w}}}\right)^{0.25} \left(1000 < Re < 2 \times 10^5\right) \tag{27}$$

$$Nu_{\mathrm{exh}} = 0.71 Re_{\mathrm{exh}}^{0.5} Pr_{\mathrm{exh}}^{0.36} \left(\frac{Pr_{\mathrm{exh}}}{Pr_{\mathrm{exh,w}}}\right)^{0.25} (Re < 1000) \tag{28}$$

The calculation formula for the heat transfer coefficient of the working fluid in the preheating section and the overheating section is determined by the Gnielinski correlation equation [63]:

$$Nu_{\mathrm{wf}} = \frac{d\alpha}{\lambda} = \frac{(f/8)(Re_{\mathrm{wf}} - 1000)Pr_{\mathrm{wf}}}{1 + 12.7\sqrt{f/8}(Pr_{\mathrm{wf}}^{2/3} - 1)} \left[1 + \left(\frac{d}{l}\right)^{2/3}\right] c_{\mathrm{t}} \tag{29}$$

The calculation formula of Darcy drag coefficient is determined by Filonenko correlation:

$$f = (1.82 \log_{10} Re_{\mathrm{wf}} - 1.64)^{-2} \tag{30}$$

In the preheating section:

$$c_{\mathrm{t}} = \left(\frac{Pr_{\mathrm{wf}}}{Pr_{\mathrm{w}}}\right)^{0.01} \left(\frac{Pr_{\mathrm{wf}}}{Pr_{\mathrm{w}}} = 0.05 \sim 20\right) \tag{31}$$

In the overheating section:

$$c_{\mathrm{t}} = \left(\frac{T_{\mathrm{wf}}}{T_{\mathrm{w}}}\right)^{0.45} \left(\frac{T_{\mathrm{wf}}}{T_{\mathrm{w}}} = 0.5 \sim 1.5\right) \tag{32}$$

Since the Liu–Winterton correlation equation can predict the heat transfer coefficient of R245fa in the two-phase section well, the heat transfer coefficient of R245fa in the two-phase section can be determined by the Liu–Winterton correlation equation [64]:

$$\alpha_{\mathrm{tp}} = \sqrt{(F\alpha_{\mathrm{fb}})^2 + (S\alpha_{\mathrm{nb}})^2} \tag{33}$$

where, $2.95 < d < 32$ mm; $568.9 < Re < 8.75 \times 10^5$

$$S = (1 + 0.055F^{0.1} Re_{\mathrm{l,i}}^{0.16})^{-1} \tag{34}$$

$$F = \left(1 + xPr_{\mathrm{l}}\left(\frac{\rho_{\mathrm{l}}}{\rho_{\mathrm{v}}} - 1\right)\right)^{0.35} \tag{35}$$

The heat transfer coefficient of film boiling is determined by the Dittus–Boelter correlation [65].

$$\alpha_{\mathrm{fb}} = 0.023(\lambda_{\mathrm{l}}/d) Re_{\mathrm{l,i}}^{0.8} Pr_{\mathrm{l}}^{0.4} \tag{36}$$

The heat transfer coefficient of nucleate boiling is determined by the Copper correlation:

$$\alpha_{\mathrm{nb}} = 55 p_{\mathrm{r}}^{0.12} {q_w}^{2/3} (-\log_{10} p_r)^{-0.55} M^{-0.5} \tag{37}$$

The heat transfer model construction process of the plate heat exchanger is:
The total heat transfer coefficient (K_{pl}) can be defined as [66]:

$$\frac{1}{K_{\mathrm{pl}}} = \frac{1}{\alpha_{\mathrm{in}}} + r_{\mathrm{in}} + \frac{\delta}{\lambda} + r_{\mathrm{out}} + \frac{1}{\alpha_{\mathrm{out}}} \tag{38}$$

The Chisholm–Wanniarachchi correlation is used to determine the heat transfer coefficient of the working fluid in the preheating section and the overheating section [67]:

$$Nu = \frac{d\alpha}{\lambda} = 0.724 \left(\frac{6\beta}{\pi}\right)^{0.646} Re^{0.583} Pr^{1/3} \tag{39}$$

$$Re = \frac{G d_{\mathrm{h}}}{\mu_{\mathrm{l}}} \left(G = \frac{\dot{m}}{Nwb};\ d_{\mathrm{h}} = \frac{4wb}{2(w+b)}\right) \tag{40}$$

The Yan–Lin correlation is used to determine the heat transfer coefficient of the working fluid in the two-phase section [67]:

$$Nu = \frac{d\alpha_{\mathrm{tp}}}{\lambda} = 1.926 {Pr_{\mathrm{l}}}^{1/3} Bo_{\mathrm{eq}}^{0.3} Re_{\mathrm{eq}}^{0.5} \left[1 - x_{\mathrm{i}} + x_{\mathrm{i}}\left(\frac{\rho_{\mathrm{l}}}{\rho_{\mathrm{v}}}\right)^{0.5}\right] \tag{41}$$

$$Re_{\mathrm{eq}} = \frac{G_{\mathrm{eq}} d_{\mathrm{h}}}{\mu_{\mathrm{l}}} \left(G_{\mathrm{eq}} = G[1 - x_{\mathrm{i}} + x_{\mathrm{i}}\left(\frac{\rho_{\mathrm{l}}}{\rho_{\mathrm{v}}}\right)^{0.5}]\right);\ Bo_{\mathrm{eq}} = \frac{q}{G_{\mathrm{eq}} r_{\mathrm{fg}}} \tag{42}$$

The heat transfer coefficient of the working fluid in the condensation section is determined by the Yin–Lio–Lin correlation [67]:

$$\alpha = 4.118\left(\frac{\lambda}{d_h}\right)Re_{eq}^{0.4}Pr_l^{1/3} \tag{43}$$

3.4. Exergy Destruction Model

Through the construction of DORCexergy model, the exergy of the system is analyzed. In HT loop, 1–2 is the expansion process of the expander. The exergy destruction during expansion ($\dot{I}_{exp,HT}$) is [68]:

$$\dot{I}_{exp,HT} = T_{env}\dot{m}_{wf,HT}(s_2 - s_1) \tag{44}$$

The heat exchange process of the preheater is 2–4. The exergy destruction of the preheater ($\dot{I}_{pre,HT}$) can be defined as:

$$\dot{I}_{pre,HT} = T_{env}\dot{m}_{wf,HT}(s_4 - s_2) + T_{env}\dot{m}_{wf,LT}(s_{L2} - s_{L4}) \tag{45}$$

The pressurization process of the working fluid pump is 4–5. Exergy destruction during pressurization ($\dot{I}_{p,HT}$) can be defined as [69]:

$$\dot{I}_{p,HT} = T_{env}\dot{m}_{wf,HT}(s_5 - s_4) \tag{46}$$

The heat exchange process of the evaporator is 5–1. The exergy destruction of the evaporator ($\dot{I}_{eva,HT}$) can be defined as:

$$\dot{I}_{eva,HT} = T_{env}\dot{m}_{wf,HT}[(s_1 - s_5) - \frac{h_1 - h_5}{T_{HT}}] \tag{47}$$

where,

$$T_{HT} = T_1 + \Delta T_{HT} \tag{48}$$

$$\Delta T_{HT} = \frac{(T_7 - T_1) - (T_8 - T_5)}{\ln\frac{T_7 - T_1}{T_8 - T_5}} \tag{49}$$

In LT loop, the work process of the expander is L1–L8. The exergy destruction of the expansion process ($\dot{I}_{exp,LT}$) is [70]:

$$\dot{I}_{exp,LT} = T_{env}\dot{m}_{wf,LT}(s_{L8} - s_{L1}) \tag{50}$$

The heat exchange process of the condenser is L8–L6. The exergy destruction of the condenser ($\dot{I}_{con.LT}$) can be defined as [71]:

$$\dot{I}_{con.LT} = T_{env}\dot{m}_{wf,LT}[(s_{L6} - s_{L8}) - \frac{h_{L6} - h_{L8}}{T_{LT}}] \tag{51}$$

where,

$$T_{LT} = T_{L6} - \Delta T_{LT} \tag{52}$$

$$\Delta T_{LT} = \frac{(T_{L8} - T_g) - (T_{L6} - T_e)}{\ln\frac{T_{L8} - T_g}{T_{L6} - T_e}} \tag{53}$$

The pressurizing process of the working fluid pump is L6–L5. Exergy destruction during pressurization ($\dot{I}_{p,LT}$) can be defined as:

$$\dot{I}_{p,LT} = T_{env}\dot{m}_{wf,LT}(s_{L5} - s_{L6}) \tag{54}$$

The heat exchange process of the intercooler is L5–L4. The exergy destruction of the intercooler ($\dot{I}_{\text{inter}}$) can be defined as [72]:

$$\dot{I}_{\text{inter}} = T_{\text{env}}\dot{m}_{\text{wf,LT}}[(s_{\text{L4}} - s_{\text{L5}}) - \frac{h_{\text{L4}} - h_{\text{L5}}}{T_{\text{inter}}}] \tag{55}$$

where,

$$T_{\text{inter}} = T_{\text{L4}} + \Delta T_{\text{inter}} \tag{56}$$

$$\Delta T_{\text{inter}} = \frac{(T_{\text{i}} - T_{\text{L4}}) - (T_{\text{h}} - T_{\text{L5}})}{\ln \frac{T_{\text{i}} - T_{\text{L4}}}{T_{\text{h}} - T_{\text{L5}}}} \tag{57}$$

The heat exchange process of the evaporator is L2–L1. The exergy destruction of the evaporation process ($\dot{I}_{\text{eva,LT}}$) can be defined as [73]:

$$\dot{I}_{\text{eva,LT}} = T_{\text{env}}\dot{m}_{\text{wf,LT}}[(s_{\text{L1}} - s_{\text{L2}}) - \frac{h_{\text{L1}} - h_{\text{L2}}}{T_{\text{cool}}}] \tag{58}$$

where,

$$T_{\text{cool}} = T_{\text{L1}} + \Delta T_{\text{cool}} \tag{59}$$

$$\Delta T_{\text{cool}} = \frac{(T_{\text{k}} - T_{\text{L1}}) - (T_{\text{j}} - T_{\text{L2}})}{\ln \frac{T_{\text{k}} - T_{\text{L1}}}{T_{\text{j}} - T_{\text{L2}}}} \tag{60}$$

Therefore, the total exergy destruction of the DORC system ($\dot{I}_{\text{tot}}$) can be defined as [74]:

$$\dot{I}_{\text{tot}} = \dot{I}_{\text{exp,HT}} + \dot{I}_{\text{pre,HT}} + \dot{I}_{\text{p,HT}} + \dot{I}_{\text{eva,HT}} + \dot{I}_{\text{exp,LT}} + \dot{I}_{\text{con.LT}} + \dot{I}_{\text{p,LT}} + \dot{I}_{\text{inter}} + \dot{I}_{\text{eva,LT}} \tag{61}$$

3.5. Economic Model

In order to evaluate the economic performance of the system, a modular costing technique is used to construct economic model of the DORC system. The bare module cost of the expander can be defined as [75,76]:

$$\log_{10} C^0_{\text{exp}} = K_{1,\text{exp}} + K_{2,\text{exp}} \log_{10} \dot{W}_{\text{exp}} + K_{3,\text{exp}} (\log_{10} \dot{W}_{\text{exp}})^2 \tag{62}$$

The bare module cost of the working fluid pump can be defined as:

$$\log_{10} C^0_{\text{P}} = K_{1,\text{P}} + K_{2,\text{P}} \log_{10} \dot{W}_{\text{P}} + K_{3,\text{P}} (\log_{10} \dot{W}_{\text{P}})^2 \tag{63}$$

The bare module cost of the fin-and-tube heat exchanger can be defined as:

$$\log_{10} C^0_{\text{ft}} = K_{1,\text{ft}} + K_{2,\text{ft}} \log A_{ft} + K_{3,\text{ft}} (\lg A_{\text{ft}})^2 \tag{64}$$

The bare module cost of the plate heat exchanger can be defined as [77]:

$$\log_{10} C^0_{\text{pl}} = K_{1,\text{pl}} + K_{2,\text{pl}} \log A_{\text{pl}} + K_{3,\text{pl}} (\lg A_{\text{pl}})^2 \tag{65}$$

The pressure correction coefficient of the working fluid pump can be defined as:

$$\log F_{\text{P,P}} = C_{1,\text{P}} + C_{2,\text{P}} \log P_{\text{P}} + C_{3,\text{P}} (\log P_{\text{P}})^2 \tag{66}$$

The pressure correction coefficient of the fin-and-tube heat exchanger can be defined as:

$$\log F_{\text{P,ft}} = C_{1,\text{ft}} + C_{2,\text{ft}} \log P_{\text{ft}} + C_{3,\text{ft}} (\log P_{\text{ft}})^2 \tag{67}$$

The pressure correction coefficient of the plate heat exchanger can be defined as:

$$\log F_{P,pl} = C_{1,pl} + C_{2,pl} \log P_{pl} + C_{3,pl} (\log P_{pl})^2 \quad (68)$$

The cost of the working fluid pump after considering the material and pressure correction factor is [78]:

$$C_P = C_P^0 (B_1 + B_2 F_{m,P} F_{P,P}) \quad (69)$$

The cost of the fin-and-tube heat exchanger after considering the material and pressure correction factor is:

$$C_{ft} = C_{ft}^0 (B_1 + B_2 F_{m,ft} F_{P,ft}) \quad (70)$$

The cost of the plate heat exchanger after considering the material and pressure correction factor is [79]:

$$C_{pl} = C_{pl}^0 \left(B_1 + B_2 F_{m,pl} F_{P,pl} \right) \quad (71)$$

F_m and F_P are pressure correction coefficients; B_1, B_2, C_1, C_2, C_3, K_1, K_2 and K_3 are cost coefficients. Table 5 shows the corresponding selected values.

Table 5. Main parameters of economic model [80].

Equipment Types	K_1	K_2	K_3	B_1	B_2	C_1	C_2	C_3	F_m
Expander	2.2659	1.4398	−0.1776	/	/	/	/	/	/
Pump	3.3892	0.0536	0.1538	1.89	1.35	−0.3935	0.3957	−0.00226	1.5
Fin-and-tube heat exchanger	4.3247	−0.3030	0.1634	1.63	1.66	0	0	0	1.25
Plate heat exchanger	4.6656	−0.1557	0.1547	0.96	1.21	0	0	0	1.0

In the model, based on the cost in 2001, the chemical engineering plant cost index (CEPCI) is used to calculate the capital cost of the equipment. Then the cost index of 2018 is used for conversion. The cost calculation formula of different components in the system is as follows [81]:

$$C_{exp,2018} = \frac{CEPCI_{2018}}{CEPCI_{2001}} C_{exp,2001} \quad (72)$$

$$C_{p,2018} = \frac{CEPCI_{2018}}{CEPCI_{2001}} C_{p,2001} \quad (73)$$

$$C_{ft,2018} = \frac{CEPCI_{2018}}{CEPCI_{2001}} C_{ft,2001} \quad (74)$$

$$C_{pl,2018} = \frac{CEPCI_{2018}}{CEPCI_{2001}} C_{pl,2001} \quad (75)$$

where,

$CEPCI_{2001}$= 397 [82]

$CEPCI_{2018}$= 648.7 [83]

Therefore, the total investment cost of the DORC system is:

$$C_{tot} = C_{exp,2018} + C_{p,2018} + C_{ft,2018} + C_{pl,2018} \quad (76)$$

In addition, the cost of operation and maintenance (COM) is 1.5% of the total cost. Capital recovery factor (CRF) can be defined as:

$$CRF = \frac{i(1+i)^{LT}}{(1+i)^{LT} - 1} \quad (77)$$

The calculation formula of electricity production cost can be defined as [84]:

$$EPC = C_{\text{tot}} \frac{CRF + f_{\text{k}}}{\left(\dot{W}_{\text{exp}} - \dot{W}_{\text{p}}\right) h_{\text{full-load}}} \tag{78}$$

Among them, f_{k} is the system operation and maintenance cost coefficient, which is 0.015. $h_{\text{full-load}}$ is the annual operating time, 8000 h. The payback time of the system (PBT) can be defined as [85]:

$$PBT = \frac{\text{In}\left(\frac{\dot{W}_{\text{net}} C_{\text{elec}} - COM}{\dot{W}_{\text{net}} C_{\text{elec}} - COM - iC_{\text{tot}}}\right)}{\text{In}(1+i)} \tag{79}$$

where the electricity price (C_{elec}) is 0.5283 \$/(kW·h) [83].

4. Results and Discussion

4.1. Validation

The thermodynamic modeling and economic modeling process of the DORC system has been verified in Ref. [31]. The isentropic efficiencies of the expander and working fluid pump in the models are 0.85 and 0.8, respectively [86,87]. The main operating parameters of DORC system are shown in Table 6.

Table 6. Selection of the main operating parameters of the DORC system.

Property	Value	Unit
P_1 [64]	2.9	MPa
ΔT_{6a-1} [31]	17	K
T_4 [88,89]	346	K
T_{L1} [88]	343	K
T_{L6} [88]	298.15	K

4.2. Thermodynamic Analysis

4.2.1. DORC System

Figure 7 shows the dynamic response characteristics of the thermal efficiency and total exergy destruction of the DORC system under full operating conditions. Figure 7a shows the dynamic response characteristics of the thermal efficiency of DORC system under full operating conditions. It can be seen from the figure that as the speed increases, the thermal efficiency of the DORC system increases first and then decreases. Starting from around 1170 r/min, the increase gradually decreases; at 1500 r/min, the thermal efficiency obtains the maximum value, which is 14.47%. As the torque increases, the thermal efficiency of the DORC system first increases and then decreases. Starting from around 430 N·m, the increase gradually decreases; at 703 N·m, the thermal efficiency obtains the maximum value, which is 14.47%. The total exergy destruction corresponding to the maximum thermal efficiency is 45.26 kW. In addition, under the rated condition of the CNG engine, the thermal efficiency of the DORC system is 14.17%. Figure 7b shows the dynamic response characteristics of the total exergy destruction of the DORC system under full operating conditions. It can be seen from the figure that as the speed increases, the total exergy destruction of the DORC system gradually increases. In high torque range, the total exergy destruction of the DORC system increases significantly. As the torque increases, the total exergy destruction of the DORC system gradually increases; in high speed range, the total exergy destruction of the DORC system increases significantly. The high total exergy destruction is distributed in high speed, high torque range. When the speed and torque are 2197 r/min and 924.2 N·m, the total exergy destruction is the greatest: 105.9 kW. Under the rated condition of CNG engine, the total exergy destruction of the DORC system is 86.08 kW. From the above analysis, it can be seen that although the thermal efficiency of the CNG engine under rated condition is 2.07% less than the maximum value under full

operating conditions, the corresponding total exergy destruction is 90.19% higher. From the perspective of thermal efficiency and total exergy destruction, for CNG engines, the rated condition is not an ideal DORC system design point.

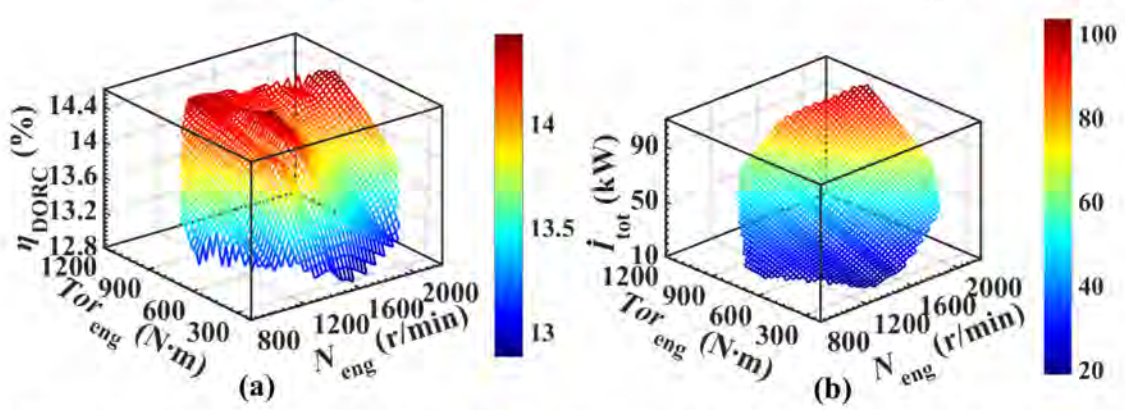

Figure 7. Dynamic response characteristics of thermal efficiency and total exergy destruction under full operating conditions. (**a**) dynamic response characteristics of the thermal efficiency of DORC system. (**b**) dynamic response characteristics of the total exergy destruction of the DORC system.

Figure 8 shows the net power output, heat exchange area, and POPA dynamic response characteristics of the DORC system under full operating conditions. Figure 8a shows the dynamic response characteristics of the net power output of the system under full operating conditions. According to the figure, as the speed increases, the net power output gradually increases; and as the torque increases, the increase gradually increases. As the torque increases, the net power output gradually increases; and with the increase of speed, the increase of net power output gradually becomes obvious. The high net power output is distributed near the rated condition. The maximum net power output is obtained under the rated condition, which is 37.54 kW. Figure 8b shows the dynamic response characteristics of the heat transfer area of the system under full operating conditions. It can be seen from the figure that the dynamic response characteristics of the heat exchange area of the system under full operating conditions are similar to the net power output. However, compared with the dynamic response characteristics of the net power output of the system, the change trend of the system heat exchange area with the speed and torque is more linear. The high heat transfer area is distributed near the rated condition. The maximum heat exchange area is obtained under the rated condition, which is 24.76 m^2.

Figure 8c shows the dynamic response characteristics of the system POPA under full operating conditions. It can be seen from the figure that as the speed increases, the POPA of the system first decreases and then increases. In low speed range, with the increase of torque, the change of POPA is not obvious. In middle speed range, as the torque increases, POPA shows an overall increasing trend. In high speed range, as the torque increases, POPA gradually decreases. High POPA is distributed in high speed, low torque range. When the speed is 1298 r/min and the torque is 500 N·m, POPA is the smallest, which is 1.16 kW/m^2. When the speed is 1997 r/min and the torque is 300 N·m, the POPA is the largest, which is 1.63 kW/m^2. Under the rated condition of the CNG engine, POPA is 1.52 kW/m^2. The POPA of CNG engine under rated condition is 6.75% less than the maximum value of POPA under full operating conditions.

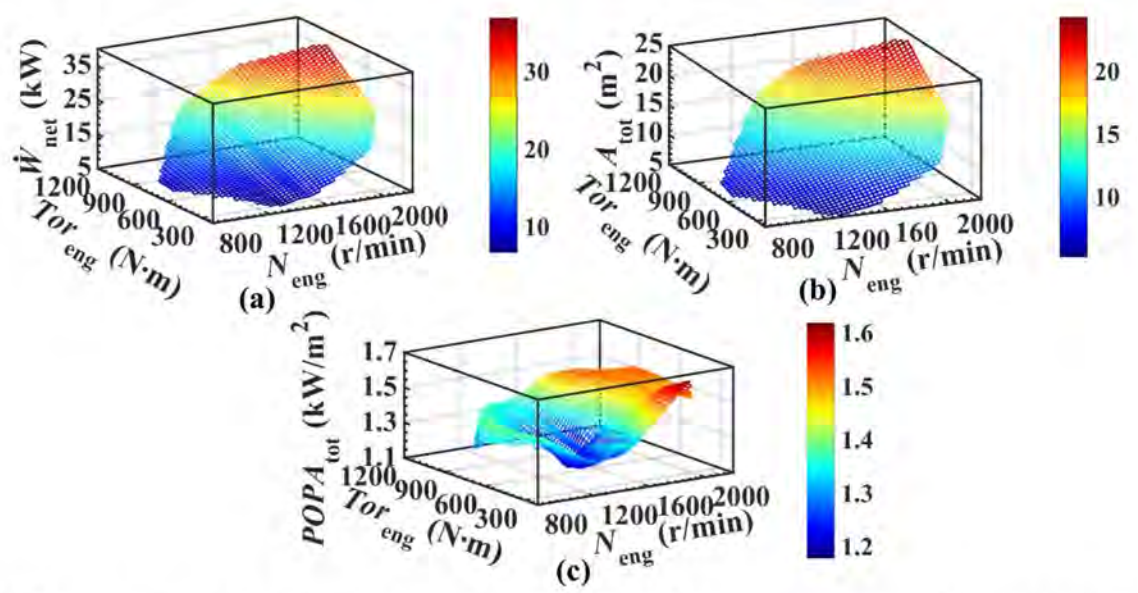

Figure 8. Dynamic response characteristics of system POPA under full operating conditions. (**a**) dynamic response characteristics of the net power output of the system. (**b**) dynamic response characteristics of the heat transfer area of the system. (**c**). dynamic response characteristics of the system POPA.

4.2.2. HT System and LT System

Figure 9 shows the dynamic response characteristics of the exergy destruction of the HT and LT loop under full operating conditions. It can be seen from the figure that the exergy destruction of the HT loop is higher than that of the LT loop under full operating conditions. The total exergy destruction of the DORC system is mainly contributed by the HT loop. In HT and LT loop, as the speed increases, the exergy destruction gradually increases. As the torque increases, the exergy destruction gradually increases; and in high speed range, the exergy destruction increases significantly. The high total exergy destruction of HT and LT loop are distributed around the rated condition. Under the rated condition, the exergy destruction of the HT and LT loop both obtain the maximum value, which are 87.77 kW and 18.13 kW, respectively.

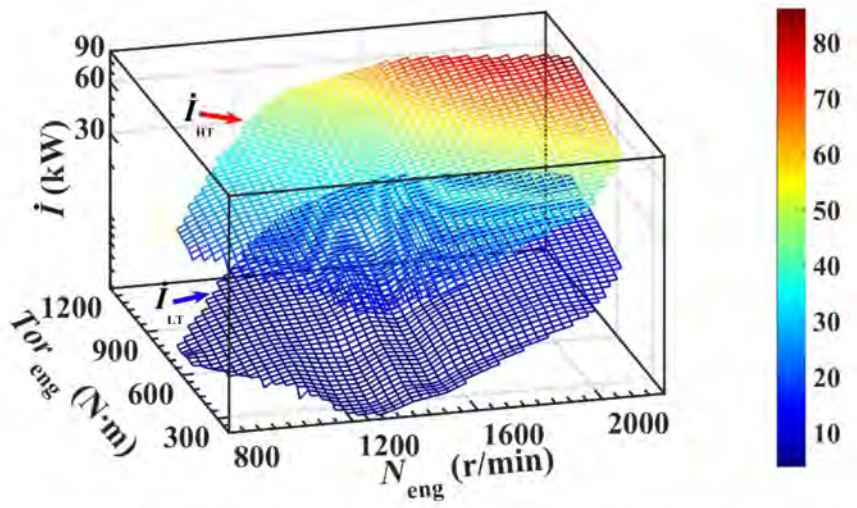

Figure 9. Dynamic response characteristics of HT loop and LT loop exergy destruction under full operating conditions.

Figure 10 shows the net power output, heat exchange area and POPA dynamic response characteristics of the HT and LT loop under full operating conditions. Figure 10a shows the dynamic response characteristics of net power output of HT and LT loop under full operating conditions. It can be seen from the figure that in HT and LT loop, as the speed increases, the net power output gradually increases; in high torque range, the increase is obvious. In HT and LT loop, as the torque increases, the net power output gradually increases; in high speed range, the increase is obvious. Under full operating conditions, the net power output of LT loop is higher than that of the HT loop. The high net power output is distributed near the rated condition. Under the rated condition, the net power output of the HT and LT loop both obtain maximum values, which are 17.06 kW and 20.48 kW, respectively.

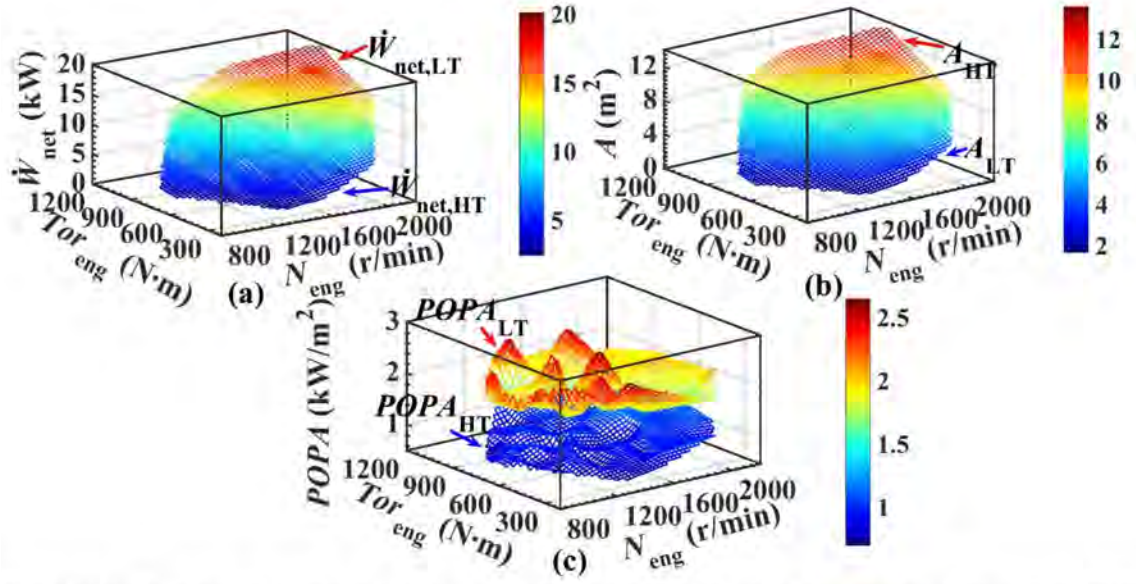

Figure 10. Dynamic response characteristics of HT loop and LT loop POPA under full operating conditions. (**a**) dynamic response characteristics of net power output of HT and LT loop. (**b**) dynamic response characteristics of the heat transfer area of the HT and LT loop. (**c**) dynamic response characteristics of POPA of the HT and LT loop.

Figure 10b shows the dynamic response characteristics of the heat transfer area of the HT and LT loop under full operating conditions. It can be seen from the figure that the dynamic response characteristics of the heat exchange area of the HT and LT loop are similar to the net power output. However, compared with the dynamic response characteristics of the net power output of the system, the heat exchange area of the HT and LT loop changes linearly with the speed and torque. Under full operating conditions, the net power output of the HT loop is higher than that of the LT loop. The high heat transfer area is distributed near the rated condition. Under the rated condition, the heat exchange area of the HT and LT loop both obtain maximum values, which are 13.82 m^2 and 10.94 m^2, respectively.

Figure 10c shows the dynamic response characteristics of POPA of the HT and LT loop under full operating conditions. It can be seen from the figure that in HT loop, as the speed increases, POPA gradually increases. In low speed range, as the torque increases, POPA does not change significantly; in high speed range, as the torque increases, POPA gradually increases. Starting from around 502 N·m, the increase gradually flat. Under the rated condition, the POPA of the HT loop is the greatest, which is 1.23 kW/m^2. In LT loop, as the speed increases, POPA shows a decreasing trend. With the increase of torque, POPA presents an obvious non-linear trend. When the speed and torque are 1399 r/min and 201 N·m respectively, the POPA of the LT loop obtains maximum value, which is 2.74 kW/m^2. Under the rated condition, the POPA of LT loop is 1.87 kW/m^2, which is 31.75% less than the maximum value.

4.2.3. Key Component

Figure 11 shows the proportion of the exergy destruction of key components to the average total exergy destruction in the DORC system. Figure 11a shows the proportion of the average exergy destruction of key components under full operating conditions. According to the figure, the exergy destruction of the evaporator in HT loop and the preheater in HT loop account for the largest proportion of the total exergy destruction; And the evaporator in HT loop and the preheater in HT loop account for the same proportion, both being 40%. In addition, in the DORC system, the working fluid pumps in HT loop and LT loop account for the least total exergy destruction, both of which do not exceed 1%. Figure 11b shows the proportion of exergy destruction of key components of the DORC system under the rated condition of the CNG engine. It can be seen from the figure that the evaporator exergy destruction in HT loop account for the largest proportion, which is 43%, and that of preheater in HT loop is the second, accounting for 37%. Similarly, in the DORC system, the working fluid pumps of HT loop and LT loop account for the least total exergy destruction, neither exceeding 1%.

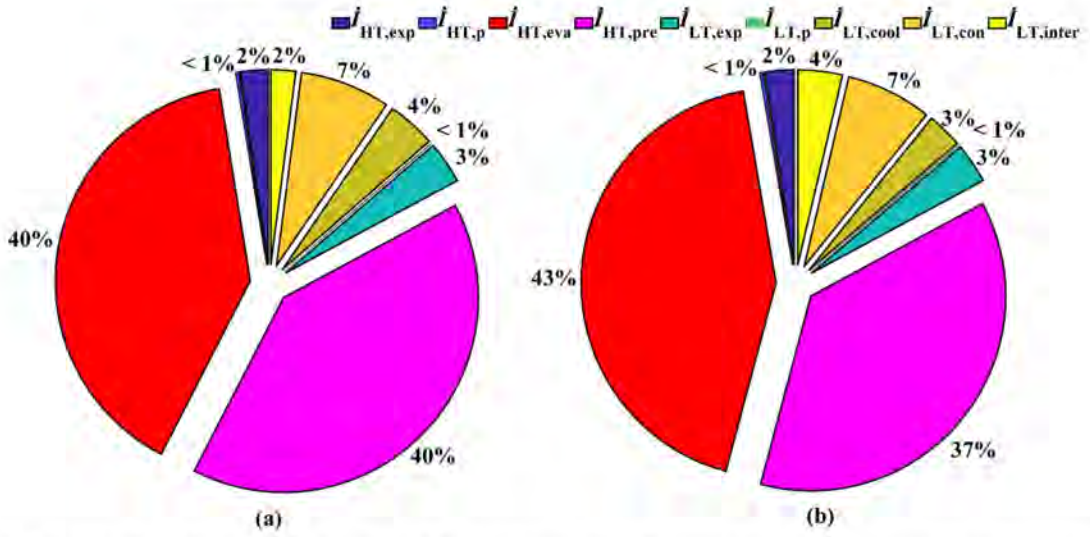

Figure 11. The proportion of exergy destruction of key components. (**a**) proportion of the average exergy destruction of key components. (**b**) proportion of exergy destruction of key components of the DORC system.

Figure 12 shows the dynamic response characteristics of the exergy destruction of key components in HT loop under full operating conditions. Figure 12a shows the dynamic response characteristics of the exergy destruction of the expander in HT loop under full operating conditions. It can be seen from the figure that as the speed increases, the exergy destruction of the expander gradually increases. at the same time, the exergy destruction increases significantly in high torque range. As the torque increases, the exergy destruction of the expander gradually increases; at the same time, the exergy destruction increases significantly in high speed range. The high exergy destruction is distributed near the rated condition of CNG. Under rated condition, the exergy destruction of the expander in HT loop obtains the maximum value, which is 2.56 kW. Figure 12b shows the dynamic response characteristics of the exergy destruction of the working fluid pump in HT loop under full operating conditions. It can be seen from the figure that the change trend of exergy destruction of the working fluid pump with speed and torque is similar to that of the expander with speed and torque in HT loop. The high exergy destruction is distributed near the rated condition. At the CNG-rated condition, the exergy destruction of the working fluid pump in HT loop obtains the maximum value, which is 0.3 kW. Figure 12c shows the dynamic response characteristics of the evaporator exergy destruction in HT loop under full operating conditions. It can be seen from the figure that the change trend of the exergy destruction of the evaporator with the speed and torque is similar to that of the expander

with the speed and torque in HT loop. The high exergy destruction is distributed near the rated condition. At the CNG rated condition, the exergy destruction of the evaporator in HT loop obtains the maximum value, which is 45.7 kW. Figure 12d shows the dynamic response characteristics of the preheater exergy destruction in HT loop under full operating conditions. It can be seen from the figure that the change trend of exergy destruction of the preheater with the speed and torque is similar to that of the expander with the speed and torque in HT loop. The high exergy destruction is distributed near the rated condition. Under the rated condition, the exergy destruction of the preheater in HT loop obtains the maximum value, which is 39.22 kW.

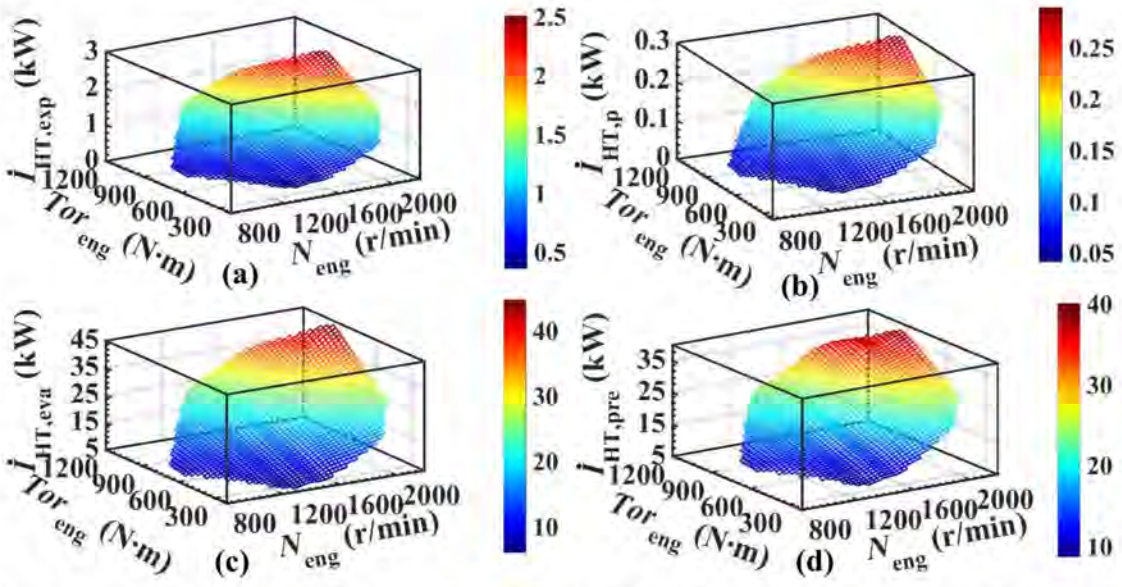

Figure 12. Dynamic response characteristics of exergy destruction of key components in HT loop under full operating conditions. (**a**) dynamic response characteristics of the exergy destruction of the expander in HT loop. (**b**) dynamic response characteristics of the exergy destruction of the working fluid pump in HT loop. (**c**) dynamic response characteristics of the evaporator exergy destruction in HT loop. (**d**) dynamic response characteristics of the preheater exergy destruction in HT loop.

Figure 13 shows the dynamic response characteristics of the exergy destruction of key components in LT loop under full operating conditions. Figure 13a shows the dynamic response characteristics of the exergy destruction of the expander in LT loop under full operating conditions. It can be seen from the figure that as the speed increases, the exergy destruction of the expander gradually increases; at the same time, in high torque range, the exergy destruction increases significantly. As the torque increases, the exergy destruction of the expander gradually increases; at the same time, the exergy destruction increases significantly in high speed range. The high exergy destruction is distributed near the rated condition. Under the rated condition, the exergy destruction of the expander in LT loop obtains the maximum value, which is 3.52 kW. Figure 13b shows the dynamic response characteristics of the exergy destruction of the working fluid pump in LT loop under full operating conditions. It can be seen from the figure that the change trend of exergy destruction of the working fluid pump with speed and torque is similar to that of the expander with the speed and torque in LT loop. The high exergy destruction is distributed near the rated condition. Under the rated condition, the exergy destruction of the working fluid pump in LT loop obtains the maximum value, which is 0.08 kW. Figure 13c shows the dynamic response characteristics of the exergy destruction of the evaporator in LT loop under full operating conditions. It can be seen from the figure that the change trend of the exergy destruction of the evaporator with the speed and torque is similar to that of the expander with the speed and torque in LT loop. The high exergy destruction is

distributed near the rated condition of CNG engine. The maximum exergy destruction of the evaporator in LT loop is 3.13 kW. Under the rated condition, the evaporator exergy destruction in LT loop is 3.11 kW, which is 0.64% less than the maximum value under full operating conditions. Figure 13d shows the dynamic response characteristics of the exergy destruction of the intercooler in LT loop under full operating conditions. It can be seen from the figure that the change trend of the exergy destruction of the intercooler with the speed and torque is similar to that of the expander with the speed and torque in LT loop. The high exergy destruction is distributed near the rated condition. Under the rated condition, the exergy destruction of the intercooler in LT loop obtains the maximum value, which is 3.91 kW. Figure 13e shows the dynamic response characteristics of the condenser exergy destruction in LT loop under full operating conditions. It can be seen from the figure that the change trend of exergy destruction of the condenser with the speed and torque is similar to that of the expander with the speed and torque in LT loop. The high exergy destruction is distributed near the rated condition. Under the rated condition, the exergy destruction of the condenser in LT loop reaches the maximum value, which is 7.52 kW.

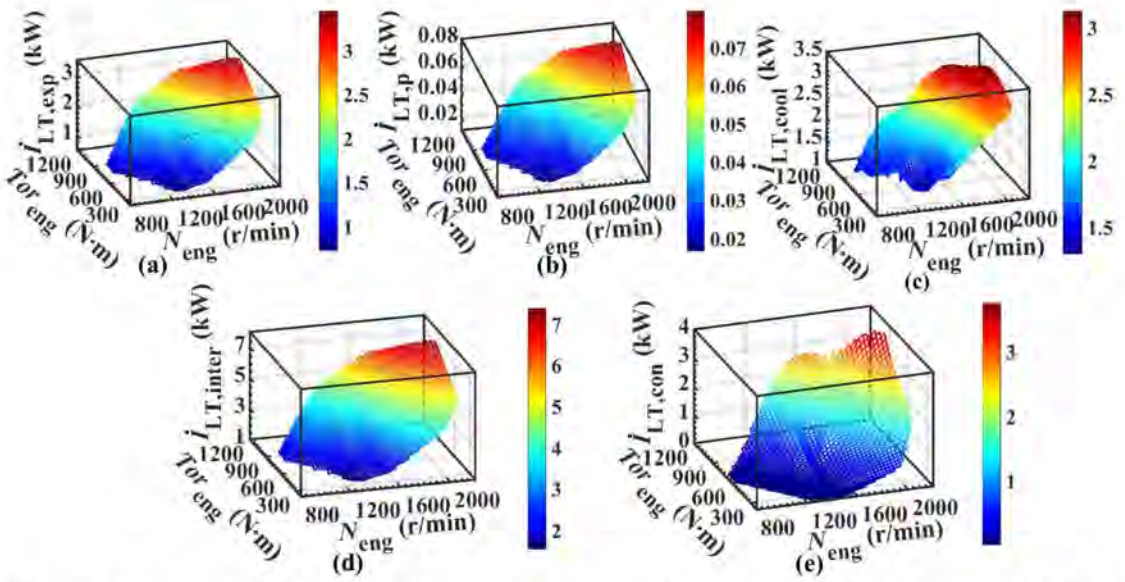

Figure 13. Dynamic response characteristics of exergy destruction of key components in LT loop under full operating conditions. (**a**) dynamic response characteristics of the exergy destruction of the expander in LT loop. (**b**). dynamic response characteristics of the exergy destruction of the working fluid pump in LT loop (**c**) dynamic response characteristics of the exergy destruction of the evaporator in LT loop. (**d**) dynamic response characteristics of the exergy destruction of the intercooler in LT loop. (**e**) dynamic response characteristics of the condenser exergy destruction in LT loop.

4.3. Economic Analysis

4.3.1. DORC System

Figure 14 shows the dynamic response characteristics of the economic performance of the DORC system under full operating conditions. Figure 14a shows the EPC dynamic response characteristics of the DORC system under full operating conditions. It can be seen from the figure that as the speed and torque increase, the EPC gradually decreases. EPC obtains the minimum value at the CNG engine rated condition, which is 0.15 $/kW·h. Figure 14b shows the PBT dynamic response characteristics of the DORC system under full operating conditions. As the speed and torque increase, PBT gradually decreases. PBT obtains the minimum value at the CNG engine rated condition, which is 3.46 years. Figure 14c shows the dynamic response characteristics of the total investment cost of the DORC system under full operating conditions. It can be seen from the figure that as the speed increases, the total investment cost gradually increases; and in high torque range, the total investment cost increases significantly. As the torque increases, the total

investment cost gradually increases; and in high speed range, the total investment cost increases significantly.

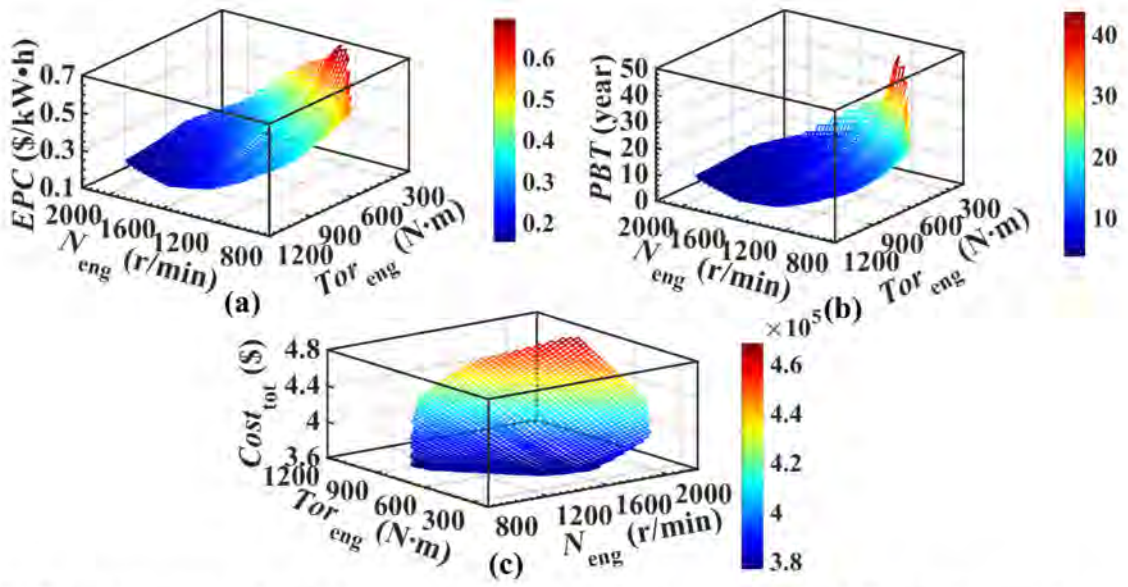

Figure 14. Dynamic response characteristics of system economic performance under full operating conditions. (**a**) EPC dynamic response characteristics of the DORC system. (**b**) PBT dynamic response characteristics of the DORC system. (**c**) dynamic response characteristics of the total investment cost of the DORC system.

4.3.2. Key Component

Figure 15 shows the dynamic response characteristics of the investment cost of key components of the DORC system under full operating condition. Figure 15a shows the dynamic response characteristics of the total investment cost of the heat exchangers under full operating conditions. It can be seen from the figure that as the speed increases, the total investment cost of the heat exchangers gradually increases; and in high torque range, the total investment cost of the heat exchangers increases significantly. As the torque increases, the total investment cost of the heat exchangers gradually increases; and in high speed range, the total investment cost of the heat exchangers increases significantly. The maximum value of the total investment cost of the heat exchangers is obtained at the CNG engine rated condition, which is 3.78 $\times$ 10^5 \$. Figure 15b shows the dynamic response characteristics of the total investment cost of the working fluid pumps under full operating conditions. It can be seen from the figure that the change trend of the total investment cost of the working fluid pumps with the speed and torque is similar to that of the heat exchangers with the speed and torque. The maximum total investment cost of the working fluid pumps is obtained at the CNG engine rated condition, which is 1.89 $\times$ 104 \$. Figure 15c shows the dynamic response characteristics of the total investment cost of the expanders under full operating conditions. It can be seen from the figure that the change trend of the total investment cost of the expanders with the speed and torque is similar to that of the heat exchangers with the speed and torque. The maximum value of the total investment cost of the expanders is obtained at the CNG engine rated condition, which is 7.43 $\times$ 104 \$.

Figure 16 shows the proportion of the investment cost of key components of the DORC system. Figure 16a shows the proportion of the average value of the total investment cost of the key components under full operating conditions. It can be seen from the figure that the total investment cost of heat exchangers accounts for the greatest proportion, which is 88%. The total investment cost of the working fluid pumps accounts for the least, which is 3%. Figure 16b shows the proportion of the investment cost of key components of the DORC system under the rated condition of CNG engine. It can be seen from the figure that

the investment cost of the heat exchangers accounts for the highest proportion, which is 80%. The investment cost of the working fluid pumps accounts for the least proportion, which is 4%.

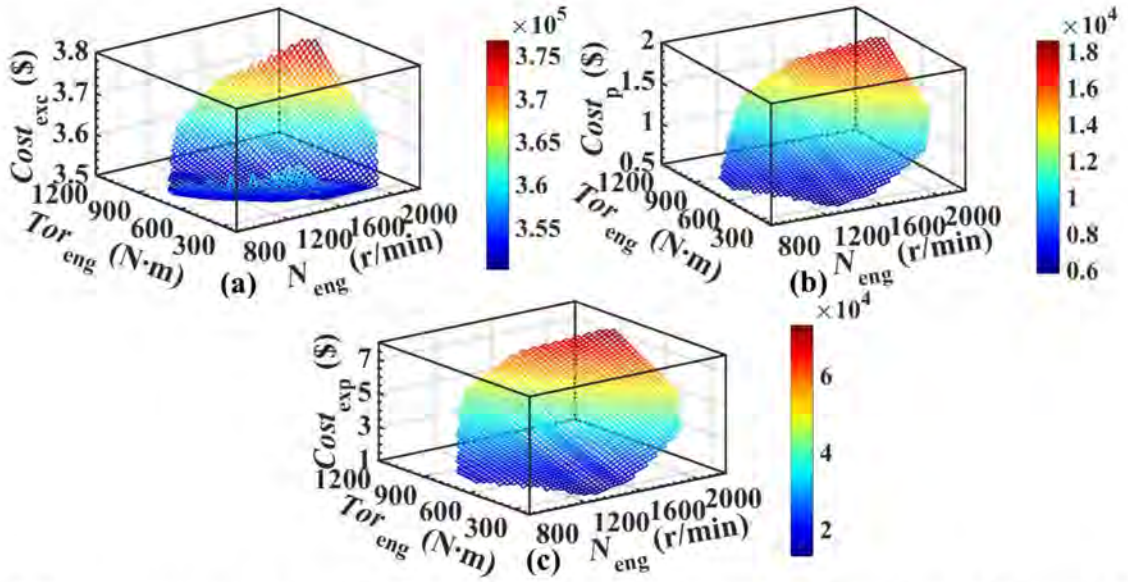

Figure 15. Dynamic response characteristics of key components total cost under full operating conditions. (**a**) dynamic response characteristics of the total investment cost of the heat exchangers. (**b**) dynamic response characteristics of the total investment cost of the working fluid pumps. (**c**) dynamic response characteristics of the total investment cost of the expanders.

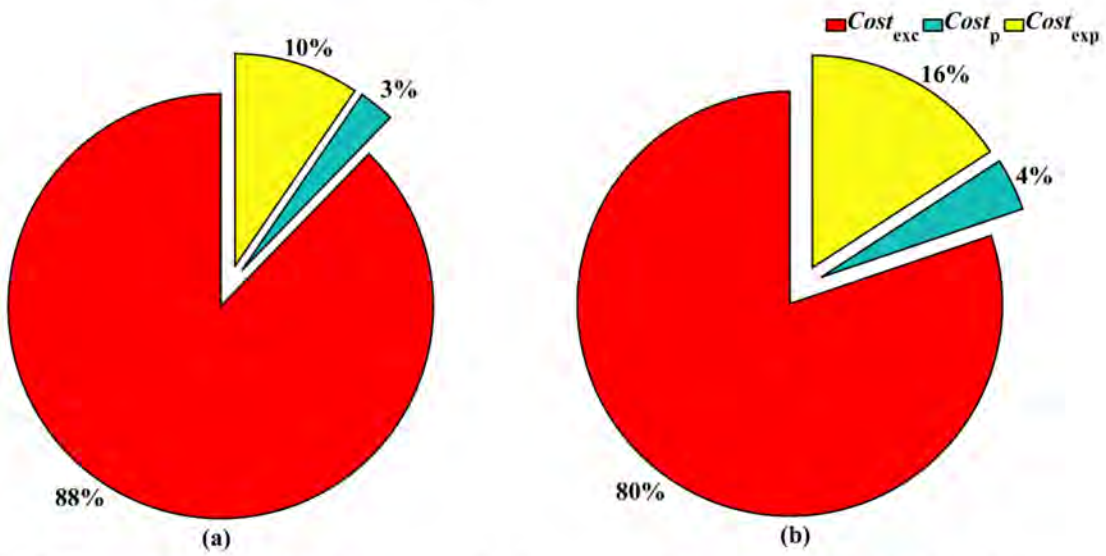

Figure 16. The proportion of cost of key components. (**a**) proportion of the average value of the total investment cost of the key components. (**b**) proportion of the investment cost of key components of the DORC system.

5. Conclusions

Based on the theory of IC engines' heat balance in high-dimensional space, this paper analyzes the dynamic characteristics of CNG engine exhaust, intercooler, and coolant waste heat sources under full operating conditions. Based on the operating characteristics of the DORC system, loops and key components, the thermodynamic models, heat transfer models and economic models are constructed respectively. In the high-dimensional space, the thermodynamic performance, heat transfer performance, and economic performance of the system, loops, and key components are analyzed and evaluated under full operating conditions of CNG engine. The main conclusions are summarized as follows:

(1) The maximum values of exhaust mass flow rate, exhaust heat transfer rate, intercooler mass flow rate, and intercooler heat transfer rate are obtained under the rated condition. In addition, the net power output and heat exchange area of the DORC system under the rated condition have the maximum values, which are 37.54 kW and 24.76 m^2, respectively. From the perspective of IC engine heat balance theory, output characteristics and heat exchange area, the CNG engine rated condition is a relatively ideal DORC system design operating point.

(2) The thermal efficiency of the DORC system under the CNG engine's rated operating conditions is 14.17%, and the corresponding total exergy loss is 86.08 kW. Although the thermal efficiency of the CNG engine under rated condition is 2.07% lower than the maximum value under full operating conditions, the corresponding total exergy destruction is 90.19% higher. The EPC and PBT at the rated condition are the minimum values, which are 0.15 $/kW·h and 3.46 years respectively.

(3) Under the rated condition of CNG engine, the total exergy destruction of HT and LT loop both obtain the maximum values, which are 87.77 kW and 18.13 kW, respectively. However, the net power output and heat exchange area of HT and LT loop also obtain the maximum values. Therefore, under the rated condition, the net power output and heat exchange area of different loops are optimal, and the loops also have the highest exergy destruction. In addition, the total exergy destruction of the DORC system is mainly contributed by the HT loop.

(4) In the HT loop, the average exergy destruction of the evaporator and the preheater accounts for the largest proportion of the average total exergy destruction, both being 40%; under the rated condition, the evaporator exergy destruction in HT loop accounts for the largest proportion, which is 43%. The average exergy destruction of the working fluid pumps account for the least of the average total exergy destruction, not exceeding 1%.

(5) The investment cost of the heat exchangers in the DORC system is the highest. Under full operating conditions, the average value of the total investment cost of the heat exchanger accounts for the average value of the total investment cost of the system is largest, which is 88%. The average value of the total investment cost of the working fluid pumps account for the average value of the total investment cost of the system is least, which is 4%.

Author Contributions: Conceptualization, B.Y.; methodology, X.P.; software, H.Z. All authors have read and agreed to the published version of the manuscript.

Funding: The National Natural Science Foundation of China (Grant No. 51776005) and the Beijing Natural Science Foundation (Grant No. 3192014), and supported by State Key Laboratory of Engines, Tianjin University (Grant No. K2020-08).

Acknowledgments: This work was sponsored by the National Natural Science Foundation of China (Grant No. 51776005) and the Beijing Natural Science Foundation (Grant No. 3192014), and supported by State Key Laboratory of Engines, Tianjin University (Grant No. K2020-08). The authors would like to thank the reviewers for their valuable comments on this research.

Conflicts of Interest: The authors declare no conflict of interest.

Nomenclature

A	heat transfer area (m^2)
Bo	boiling number
b	channel spacing (m)
C_p	specific heat at constant pressure
c_t	temperature difference correction factor
d	diameter (m)
F	forced convective heat transfer enhancement factor
f	Darcy resistance coefficient
G	mass velocity ($kg/m^2 \cdot s$)
H	fuel low calorific value
h	specific enthalpy (kJ/kg)
I	exergy destruction (kW)
i	annual interest rate
K	overall heat transfer coefficient ($W/m^2 \cdot K$)
LT	lifetime (years)
l	length (m)
M	molecular weight (kg/kmol)
$\dot{m}$	mass flow rate (kg/s)
Nu	Nusselt number
P	pressure (MPa)
p_r	reduced pressure
Pr	Prandtl number
$\dot{Q}$	heat transfer rate (kW)
q	heat flux ($kW/(m^2 \cdot K)$)
r_{fg}	enthalpy of vaporization (J/kg)
Re	Reynolds number
S	suppression factor
s	specific entropy
T	temperature (K)
$\dot{W}$	power output (kW)
w	channel width (m)
x	mass fraction
Greek letters	
η	thermal efficiency
λ	thermal conductivity ($W/m \cdot K$)
β	rib effect coefficient
r	fouling resistance ($m^2 \cdot K/W$)
ε	correction factor
δ	fin height (m)
α	heat transfer coefficient ($W/m^2 \cdot K$)
μ	dynamic viscosity ($N \cdot s/m^2$)
Subscripts/Subscripts	
cool	coolant
env	environment
eng	engine
exh	exhaust
eva	evaporator
exp	expander
eq	equivalent
f	fin
ft	fin-and-tube heat exchanger
fb	film boiling
h	hydraulic
in	inner
inter	intercooler
l	liquid

LT	lifetime or low temperature
nb	nucleate boiling
th	thermal
tp	two-phase
tot	total
out	outer
P	pressure (MPa) or pump
pl	plate heat exchanger
pre	preheater
tot	total
v	vapor
w	wall
wf	working fluid
6a-1	state points in HT loop

Acronyms

CNG	compressed natural gas
DORC	dual loop organic Rankine cycle
EPC	electricity production cost
HT	high temperature
IC	internal combustion
LT	low temperature
LMTD	logarithmic mean temperature difference
ORC	organic Rankine cycle
PBT	payback time
POPA	net power output per unit heat transfer area
WHR	waste heat recovery

References

1. Li, M.; Wu, H.; Zhang, T.; Shen, B.; Zhang, Q.; Li, Z. A comprehensive review of pilot ignited high pressure direct injection natural gas engines: Factors affecting combustion, emissions and performance. *Renew. Sustain. Energy Rev.* **2019**, *119*, 109653. [CrossRef]
2. Prasad, R.K.; Mustafi, N.; Agarwal, A.K. Effect of spark timing on laser ignition and spark ignition modes in a hydrogen enriched compressed natural gas fuelled engine. *Fuel* **2020**, *276*, 11807. [CrossRef]
3. Lee, C.-F.; Pang, Y.; Wu, H.; Hernández, J.J.; Zhang, S.; Liu, F. An optical investigation of substitution rates on natural gas/diesel dual-fuel combustion in a diesel engine. *Appl. Energy* **2020**, *261*, 114455. [CrossRef]
4. Ping, X.; Yang, F.; Zhang, H.; Zhang, W.; Zhang, J.; Song, G.; Wang, C.; Yao, B.; Wu, Y. Prediction and optimization of power output of single screw expander in organic Rankine cycle (ORC) for diesel engine waste heat recovery. *Appl. Therm. Eng.* **2020**, *182*, 116048. [CrossRef]
5. Yang, F.; Cho, H.; Zhang, H.; Zhang, J.; Wu, Y. Artificial neural network (ANN) based prediction and optimization of an organic Rankine cycle (ORC) for diesel engine waste heat recovery. *Energy Convers. Manag.* **2018**, *164*, 15–26. [CrossRef]
6. Ping, X.; Yang, F.; Zhang, H.; Zhang, W.; Song, G.; Yang, Y. Prediction and optimization of isentropic efficiency of vortex pump under full operating conditions in Organic Rankine Cycle waste heat recovery system based on deep learning and intelligent algorithm. *Sustain. Energy Technol. Assess.* **2020**, *42*, 100898.
7. Wang, E.; Yu, Z.; Zhang, H.; Yang, F. A regenerative supercritical-subcritical dual-loop organic Rankine cycle system for energy recovery from the waste heat of internal combustion engines. *Appl. Energy* **2017**, *190*, 574–590. [CrossRef]
8. Wu, X.; Chen, J.; Xie, L. Optimal design of organic Rankine cycles for exhaust heat recovery from light-duty vehicles in view of various exhaust gas conditions and negative aspects of mobile vehicles. *Appl. Therm. Eng.* **2020**, *179*, 115645. [CrossRef]
9. Xie, H.; Yang, C. Dynamic behavior of Rankine cycle system for waste heat recovery of heavy duty diesel engines under driving cycle. *Appl. Energy* **2013**, *112*, 130–141. [CrossRef]
10. Wang, C.; Yang, F.; Zhang, H.; Zhao, R.; Xu, Y. Energy recovery efficiency analysis of organic Rankine cycle system in vehicle engine under different road conditions. *Energy Convers. Manag.* **2020**, *223*, 113317. [CrossRef]
11. Shu, G.; Zhao, M.; Tian, H.; Wei, H.; Liang, X.; Huo, Y.; Zhu, W. Experimental investigation on thermal OS/ORC (Oil Storage/Organic Rankine Cycle) system for waste heat recovery from diesel engine. *Energy* **2016**, *107*, 693–706. [CrossRef]
12. Zhai, H.; An, Q.; Shi, L.; Lemort, V.; Quoilin, S. Categorization and analysis of heat sources for organic Rankine cycle systems. *Renew. Sustain. Energy Rev.* **2016**, *64*, 790–805. [CrossRef]
13. Boyaghchi, F.A.; Chavoshi, M. Monthly assessments of exergetic, economic and environmental criteria and optimization of a solar micro-CCHP based on DORC. *Sol. Energy* **2018**, *166*, 351–370. [CrossRef]

14. Wang, X.; Shu, G.; Tian, H.; Liu, P.; Jing, D.; Li, X. Dynamic analysis of the dual-loop Organic Rankine Cycle for waste heat recovery of a natural gas engine. *Energy Convers. Manag.* **2017**, *148*, 724–736. [CrossRef]
15. Huang, H.; Zhu, J.; Yan, B. Comparison of the performance of two different Dual-loop organic Rankine cycles (DORC) with nanofluid for engine waste heat recovery. *Energy Convers. Manag.* **2016**, *126*, 99–109. [CrossRef]
16. Rostamzadeh, H.; Ghaebi, H.; Vosoughi, S.; Jannatkhah, J. Thermodynamic and thermoeconomic analysis and optimization of a novel dual-loop power/refrigeration cycle. *Appl. Therm. Eng.* **2018**, *138*, 1–17. [CrossRef]
17. Baldasso, E.; Mondejar, M.E.; Andreasen, J.G.; Rønnenfelt, K.A.T.; Nielsen, B.; Haglind, F. Design of organic Rankine cycle power systems for maritime applications accounting for engine backpressure effects. *Appl. Therm. Eng.* **2020**, *178*, 115527. [CrossRef]
18. Wang, Z.; Hu, Y.; Xia, X.; Zuo, Q.; Zhao, B.; Li, Z. Thermo-economic selection criteria of working fluid used in dual-loop ORC for engine waste heat recovery by multi-objective optimization. *Energy* **2020**, *197*, 117053. [CrossRef]
19. Zhi, L.-H.; Hu, P.; Chen, L.-X.; Zhao, G. Performance analysis and optimization of engine waste heat recovery with an improved transcritical-subcritical parallel organic Rankine cycle based on zeotropic mixtures. *Appl. Therm. Eng.* **2020**, *181*, 115991. [CrossRef]
20. Zhi, L.-H.; Hu, P.; Chen, L.-X.; Zhao, G. Thermodynamic analysis of an innovative transcritical CO_2 parallel Rankine cycle driven by engine waste heat and liquefied natural gas cold. *Energy Convers. Manag.* **2020**, *209*, 112583. [CrossRef]
21. Song, J.; Li, X.; Wang, K.; Markides, C.N. Parametric optimisation of a combined supercritical CO_2 (S-CO_2) cycle and organic Rankine cycle (ORC) system for internal combustion engine (ICE) waste-heat recovery. *Energy Convers. Manag.* **2020**, *218*, 112999. [CrossRef]
22. Zhi, L.-H.; Hu, P.; Chen, L.-X.; Zhao, G. Thermodynamic analysis of a novel transcritical-subcritical parallel organic Rankine cycle system for engine waste heat recovery. *Energy Convers. Manag.* **2019**, *197*, 111855. [CrossRef]
23. Fang, Y.; Yang, F.; Zhang, H. Comparative analysis and multi-objective optimization of organic Rankine cycle (ORC) using pure working fluids and their zeotropic mixtures for diesel engine waste heat recovery. *Appl. Therm. Eng.* **2019**, *157*, 113704. [CrossRef]
24. Nawi, Z.M.; Kamarudin, S.; Abdullah, S.S.; Lam, S.S. The potential of exhaust waste heat recovery (WHR) from marine diesel engines via organic rankine cycle. *Energy* **2018**, *166*, 17–31. [CrossRef]
25. Shu, G.; Wang, X.; Tian, H.; Liu, P.; Jing, D.; Li, X. Scan of working fluids based on dynamic response characters for Organic Rankine Cycle using for engine waste heat recovery. *Energy* **2017**, *133*, 609–620. [CrossRef]
26. Chen, T.; Zhuge, W.; Zhang, Y.; Zhang, L. A novel cascade organic Rankine cycle (ORC) system for waste heat recovery of truck diesel engines. *Energy Convers. Manag.* **2017**, *138*, 210–223. [CrossRef]
27. Seyedkavoosi, S.; Javan, S.; Kota, K. Exergy-based optimization of an organic Rankine cycle (ORC) for waste heat recovery from an internal combustion engine (ICE). *Appl. Therm. Eng.* **2017**, *126*, 447–457. [CrossRef]
28. Kim, Y.M.; Gil Shin, D.; Kim, C.G.; Cho, G.B. Single-loop organic Rankine cycles for engine waste heat recovery using both low- and high-temperature heat sources. *Energy* **2016**, *96*, 482–494. [CrossRef]
29. Neto, R.D.O.; Sotomonte, C.A.R.; Coronado, C.J.; Nascimento, M.A. Technical and economic analyses of waste heat energy recovery from internal combustion engines by the Organic Rankine Cycle. *Energy Convers. Manag.* **2016**, *129*, 168–179. [CrossRef]
30. Shi, L.; Shu, G.; Tian, H.; Deng, S. A review of modified Organic Rankine cycles (ORCs) for internal combustion engine waste heat recovery (ICE-WHR). *Renew. Sustain. Energy Rev.* **2018**, *92*, 95–110. [CrossRef]
31. Yang, F.; Zhang, H.; Yu, Z.; Wang, E.; Meng, F.; Liu, H.; Wang, J.; Yang, F.; Zhang, H.; Yu, Z.; et al. Parametric optimization and heat transfer analysis of a dual loop ORC (organic Rankine cycle) system for CNG engine waste heat recovery. *Energy* **2017**, *118*, 753–775. [CrossRef]
32. Wang, Z.Q.; Xia, X.X.; Pan, H.H.; Zuo, Q.S.; Zhou, N.J.; Xie, B.Q. Fluid selection and advanced exergy analysis of dual-loop ORC using zeotropic mixture. *Appl. Therm. Eng.* **2021**, *185*, 116423. [CrossRef]
33. Fouad, W.A. A combined heat, hydrogen and power tri-generation system based on the use of catalytic membrane reactors with a dual-loop organic Rankine cycle. *Energy Convers. Manag.* **2020**, *222*, 113255. [CrossRef]
34. Linnemann, M.; Priebe, K.-P.; Heim, A.; Wolff, C.; Vrabec, J. Experimental investigation of a cascaded organic Rankine cycle plant for the utilization of waste heat at high and low temperature levels. *Energy Convers. Manag.* **2020**, *205*, 112381. [CrossRef]
35. Liu, X.; Nguyen, M.Q.; He, M. Performance analysis and optimization of an electricity-cooling cogeneration system for waste heat recovery of marine engine. *Energy Convers. Manag.* **2020**, *214*, 112887. [CrossRef]
36. Surendran, A.; Seshadri, S. Performance investigation of two stage Organic Rankine Cycle (ORC) architectures using induction turbine layouts in dual source waste heat recovery. *Energy Convers. Manag. X* **2020**, *6*, 100029. [CrossRef]
37. Ebadollahi, M.; Rostamzadeh, H.; Seyedmatin, P.; Ghaebi, H.; Amidpour, M. Thermal and exergetic performance enhancement of basic dual-loop combined cooling and power cycle driven by solar energy. *Therm. Sci. Eng. Prog.* **2020**, *18*, 100556. [CrossRef]
38. Pourpasha, H.; Mohammadfam, Y.; Khani, L.; Mohammadpourfard, M.; Heris, S.Z. Thermodynamic and thermoeconomic analyses of a new dual-loop organic Rankine—Generator absorber heat exchanger power and cooling cogeneration system. *Energy Convers. Manag.* **2020**, *224*, 113356. [CrossRef]
39. Emadi, M.A.; Chitgar, N.; Oyewunmi, O.A.; Markides, C. Working-fluid selection and thermoeconomic optimisation of a combined cycle cogeneration dual-loop organic Rankine cycle (ORC) system for solid oxide fuel cell (SOFC) waste-heat recovery. *Appl. Energy* **2020**, *261*, 114384. [CrossRef]
40. Xia, X.X.; Wang, Z.Q.; Zhou, N.J.; Hu, Y.H.; Zhang, J.P.; Chen, Y. Working fluid selection of dual-loop organic Rankine cycle using multi-objective optimization and improved grey relational analysis. *Appl. Therm. Eng.* **2020**, *171*, 115028. [CrossRef]

41. Mohammadkhani, F.; Yari, M. A 0D model for diesel engine simulation and employing a transcritical dual loop Organic Rankine Cycle (ORC) for waste heat recovery from its exhaust and coolant: Thermodynamic and economic analysis. *Appl. Therm. Eng.* **2019**, *150*, 329–347. [CrossRef]
42. Ouyang, T.; Su, Z.; Huang, G.; Zhao, Z.; Wang, Z.; Chen, N.; Huang, H. Modeling and optimization of a combined cooling, cascaded power and flue gas purification system in marine diesel engines. *Energy Convers. Manag.* **2019**, *200*, 112102. [CrossRef]
43. Liang, Y.; Bian, X.; Qian, W.; Pan, M.; Ban, Z.; Yu, Z. Theoretical analysis of a regenerative supercritical carbon dioxide Brayton cycle/organic Rankine cycle dual loop for waste heat recovery of a diesel/natural gas dual-fuel engine. *Energy Convers. Manag.* **2019**, *197*, 111845. [CrossRef]
44. Huang, H.; Zhu, J.; Deng, W.; Ouyang, T.; Yan, B.; Yang, X. Influence of exhaust heat distribution on the performance of dual-loop organic Rankine Cycles (DORC) for engine waste heat recovery. *Energy* **2018**, *151*, 54–65. [CrossRef]
45. Ebrahimi, K.; Jones, G.F.; Fleischer, A.S. The viability of ultra low temperature waste heat recovery using organic Rankine cycle in dual loop data center applications. *Appl. Therm. Eng.* **2017**, *126*, 393–406. [CrossRef]
46. Usman, M.; Imran, M.; Yang, Y.; Lee, D.H.; Park, B.-S. Thermo-economic comparison of air-cooled and cooling tower based Organic Rankine Cycle (ORC) with R245fa and R1233zde as candidate working fluids for different geographical climate conditions. *Energy* **2017**, *123*, 353–366. [CrossRef]
47. Lim, T.-W.; Choi, Y.-S.; Hwang, D.-H. Optimal working fluids and economic estimation for both double stage organic Rankine cycle and added double stage organic Rankine cycle used for waste heat recovery from liquefied natural gas fueled ships. *Energy Convers. Manag.* **2021**, *242*, 114323. [CrossRef]
48. Zhang, Y.-Q.; Wu, Y.; Xia, G.; Ma, C.-F.; Ji, W.-N.; Liu, S.-W.; Yang, K.; Yang, F.-B. Development and experimental study on organic Rankine cycle system with single-screw expander for waste heat recovery from exhaust of diesel engine. *Energy* **2014**, *77*, 499–508. [CrossRef]
49. Yang, S.-C.; Hung, T.-C.; Feng, Y.-Q.; Wu, C.-J.; Wong, K.-W.; Huang, K.-C. Experimental investigation on a 3 kW organic Rankine cycle for low-grade waste heat under different operation parameters. *Appl. Therm. Eng.* **2017**, *113*, 756–764. [CrossRef]
50. Ping, X.; Yang, F.; Zhang, H.; Zhang, J.; Zhang, W.; Song, G. Introducing machine learning and hybrid algorithm for prediction and optimization of multistage centrifugal pump in an ORC system. *Energy* **2021**, *222*, 120007. [CrossRef]
51. Mohammadi, K.; Ellingwood, K.; Powell, K. A novel triple power cycle featuring a gas turbine cycle with supercritical carbon dioxide and organic Rankine cycles: Thermoeconomic analysis and optimization. *Energy Convers. Manag.* **2020**, *220*, 113123. [CrossRef]
52. Fernández-Guillamón, A.; Molina-García, A.; Vera-García, F.; Almendros-Ibáñez, J. Organic Rankine Cycle Optimization Performance Analysis Based on Super-Heater Pressure: Comparison of Working Fluids. *Energies* **2021**, *14*, 2548. [CrossRef]
53. Ping, X.; Yao, B.; Zhang, H.; Yang, F. Thermodynamic, economic, and environmental analysis and multi-objective optimization of a dual loop organic Rankine cycle for CNG engine waste heat recovery. *Appl. Therm. Eng.* **2021**, *193*, 116980. [CrossRef]
54. Kuric, I.; Klačková, I.; Nikitin, Y.; Zajačko, I.; Císar, M.; Tucki, K. Analysis of Diagnostic Methods and Energy of Production Systems Drives. *Processes* **2021**, *9*, 843. [CrossRef]
55. Tjahjono, T.; Ehyaei, M.; Ahmadi, A.; Hoseinzadeh, S.; Memon, S. Thermo-Economic Analysis on Integrated CO_2, Organic Rankine Cycles, and NaClO Plant Using Liquefied Natural Gas. *Energies* **2021**, *14*, 2849. [CrossRef]
56. Eppinger, B.; Muradi, M.; Scharrer, D.; Zigan, L.; Bazan, P.; German, R.; Will, S. Simulation of the Part Load Behavior of Combined Heat Pump-Organic Rankine Cycle Systems. *Energies* **2021**, *14*, 3870. [CrossRef]
57. Figiel, A.; Klačková, I. Safety requirements for mining systems controlled in automatic mode. *Tech. Univ. Kosice* **2020**, *25*, 417–426. [CrossRef]
58. Quoilin, S.; Lemort, V.; Lebrun, J. Experimental study and modeling of an Organic Rankine Cycle using scroll expander. *Appl. Energy* **2010**, *87*, 1260–1268. [CrossRef]
59. Li, M.; Wang, J.; Li, S.; Wang, X.; He, W.; Dai, Y. Thermo-economic analysis and comparison of a CO_2 transcritical power cycle and an organic Rankine cycle. *Geothermics* **2014**, *50*, 101–111. [CrossRef]
60. Li, X.; Song, J.; Yu, G.; Liang, Y.; Tian, H.; Shu, G.; Markides, C.N. Organic Rankine cycle systems for engine waste-heat recovery: Heat exchanger design in space-constrained applications. *Energy Convers. Manag.* **2019**, *199*, 111968. [CrossRef]
61. Zhang, H.; Wang, E.; Fan, B. Heat transfer analysis of a finned-tube evaporator for engine exhaust heat recovery. *Energy Convers. Manag.* **2013**, *65*, 438–447. [CrossRef]
62. Zukauskas, A. Heat Transfer from Tubes in Crossflow. *Adv. Heat Transf.* **1972**, *8*, 93–160.
63. Gnielinski, V. New equations for heat mass transfer in turbulent pipe and channel flows. *Int. J. Chem. Eng.* **1976**, *16*, 359–368.
64. Liu, Z.; Winterton, R. A general correlation for saturated and subcooled flow boiling in tubes and annuli, based on a nucleate pool boiling equation. *Int. J. Heat Mass Transf.* **1991**, *34*, 2759–2766. [CrossRef]
65. Ghiaasiaan, S.M. *Two-Phase Flow, Boiling and Condensation in Conventional and Miniature Systems*; Cambridge University Press: Cambridge, UK, 2008; pp. 321–353.
66. Zhao, Y.; Wang, J. Exergoeconomic analysis and optimization of a flash-binary geothermal power system. *Appl. Energy* **2016**, *179*, 159–170. [CrossRef]
67. García-Cascales, J.R.; Vera-García, F.; Corberan, J.M.; Maciá, J.G. Assessment of boiling and condensation heat transfer correlations in the modelling of plate heat exchangers. *Int. J. Refrig.* **2007**, *30*, 1029–1041. [CrossRef]

68. Lu, Y.; Roskilly, A.P.; Tang, K.; Wang, Y.; Jiang, L.; Yuan, Y.; Wang, L. Investigation and performance study of a dual-source chemisorption power generation cycle using scroll expander. *Appl. Energy* **2017**, *204*, 979–999. [CrossRef]
69. Ramli, W.R.B.W.; Pesyridis, A.; Gohil, D.; Alshammari, F. Organic Rankine Cycle Waste Heat Recovery for Passenger Hybrid Electric Vehicles. *Energies* **2020**, *13*, 4532. [CrossRef]
70. Fatigati, F.; Vittorini, D.; Wang, Y.; Song, J.; Markides, C.N.; Cipollone, R. Design and Operational Control Strategy for Optimum Off-Design Performance of an ORC Plant for Low-Grade Waste Heat Recovery. *Energies* **2020**, *13*, 5846. [CrossRef]
71. Abam, F.; Diemuodeke, O.; Ekwe, E.; Alghassab, M.; Samuel, O.; Khan, Z.; Imran, M.; Farooq, M. Exergoeconomic and Environmental Modeling of Integrated Polygeneration Power Plant with Biomass-Based Syngas Supplemental Firing. *Energies* **2020**, *13*, 6018. [CrossRef]
72. Wang, E.; Zhang, H.; Fan, B.; Ouyang, M.; Yang, F.; Yang, K.; Wang, Z.; Zhang, J. Parametric analysis of a dual-loop ORC system for waste heat recovery of a diesel engine. *Appl. Therm. Eng.* **2014**, *67*, 168–178. [CrossRef]
73. Ping, X.; Yao, B.; Zhang, H.; Yang, F. Thermodynamic analysis and high-dimensional evolutionary many-objective optimization of dual loop organic Rankine cycle (DORC) for CNG engine waste heat recovery. *Energy* **2021**, *236*, 121508. [CrossRef]
74. Tian, H.; Chang, L.; Gao, Y.; Shu, G.; Zhao, M.; Yan, N. Thermo-economic analysis of zeotropic mixtures based on siloxanes for engine waste heat recovery using a dual-loop organic Rankine cycle (DORC). *Energy Convers. Manag.* **2017**, *136*, 11–26. [CrossRef]
75. Akatov, N.; Mingaleva, Z.; Klačková, I.; Galieva, G.; Shaidurova, N. Expert Technology for Risk Management in the Implementation of QRM in a High-Tech Industrial Enterprise. *Manag. Syst. Prod. Eng.* **2019**, *27*, 250–254. [CrossRef]
76. Esfandi, S.; Baloochzadeh, S.; Asayesh, M.; Ehyaei, M.A.; Ahmadi, A.; Rabanian, A.A.; Das, B.; Costa, V.A.F.; Davarpanah, A. Energy, Exergy, Economic, and Exergoenvironmental Analyses of a Novel Hybrid System to Produce Electricity, Cooling, and Syngas. *Energies* **2020**, *13*, 6453. [CrossRef]
77. Pascale, A.D. Organic Rankine Cycle for Energy Recovery System. *Energies* **2021**, *14*, 5253. [CrossRef]
78. Andreasen, J.G.; Baldasso, E.; Kærn, M.R.; Weith, T.; Heberle, F.; Brüggemann, D.; Haglind, F. Techno-economic feasibility analysis of zeotropic mixtures and pure fluids for organic Rankine cycle systems. *Appl. Therm. Eng.* **2021**, *192*, 116791. [CrossRef]
79. Steger, D.; Regensburger, C.; Pham, J.; Schlucker, E. Heat Exchangers in Carnot Batteries: Condensation and Evaporation in a Reversible Device. *Energies* **2021**, *14*, 5620. [CrossRef]
80. Yang, M.-H.; Yeh, R.-H. Thermodynamic and economic performances optimization of an organic Rankine cycle system utilizing exhaust gas of a large marine diesel engine. *Appl. Energy* **2015**, *149*, 1–12. [CrossRef]
81. Holubčík, M.; Klačková, I.; Ďurčanský, P. Pyrolysis Conversion of Polymer Wastes to Noble Fuels in Conditions of the Slovak Republic. *Energies* **2020**, *13*, 4849. [CrossRef]
82. Zhang, C.; Liu, C.; Wang, S.; Xu, X.; Li, Q. Thermo-economic comparison of subcritical organic Rankine cycle based on different heat exchanger configurations. *Energy* **2017**, *123*, 728–741. [CrossRef]
83. Li, T.; Liu, Q.; Xu, Y.; Dong, Z.; Meng, N.; Jia, Y.; Qin, H. Techno-economic performance of multi-generation energy system driven by associated mixture of oil and geothermal water for oilfield in high water cut. *Geothermics* **2020**, *89*, 101991. [CrossRef]
84. Fergani, Z.; Morosuk, T.; Touil, D. Exergy-Based Multi-Objective Optimization of an Organic Rankine Cycle with a Zeotropic Mixture. *Entropy* **2021**, *23*, 954. [CrossRef] [PubMed]
85. Oyekale, J.; Petrollese, M.; Heberle, F.; Brüggemann, D.; Cau, G. Exergetic and integrated exergoeconomic assessments of a hybrid solar-biomass organic Rankine cycle cogeneration plant. *Energy Convers. Manag.* **2020**, *215*, 112905. [CrossRef]
86. Wang, E.; Zhang, H.; Zhao, Y.; Fan, B.; Wu, Y.; Mu, Q. Performance analysis of a novel system combining a dual loop organic Rankine cycle (ORC) with a gasoline engine. *Energy* **2012**, *43*, 385–395. [CrossRef]
87. Li, G. Organic Rankine cycle performance evaluation and thermoeconomic assessment with various applications part II: Economic assessment aspect. *Renew. Sustain. Energy Rev.* **2016**, *64*, 490–505. [CrossRef]
88. Shu, G.; Yu, G.; Tian, H.; Wei, H.; Liang, X.; Huang, Z. Multi-approach evaluations of a cascade-Organic Rankine Cycle (C-ORC) system driven by diesel engine waste heat: Part A—Thermodynamic evaluations. *Energy Convers. Manag.* **2016**, *108*, 579–595. [CrossRef]
89. Shu, G.; Liu, L.; Tian, H.; Wei, H.; Xu, X. Performance comparison and working fluid analysis of subcritical and transcritical dual-loop organic Rankine cycle (DORC) used in engine waste heat recovery. *Energy Convers. Manag.* **2013**, *74*, 35–43. [CrossRef]